5 Results and Discussions

5.1 Pre-formulation Studies

5.1.1 HPLC analytical method development

The calibration curves of LP were prepared by using methanol for LP (for *in-vitro* samples) and plasma (for *in-vivo* samples) as solvents. The curves of LP in methanol and plasma and their respective R^2 values are given in **Figure 5.1** and **Figure 5.2**, respectively.

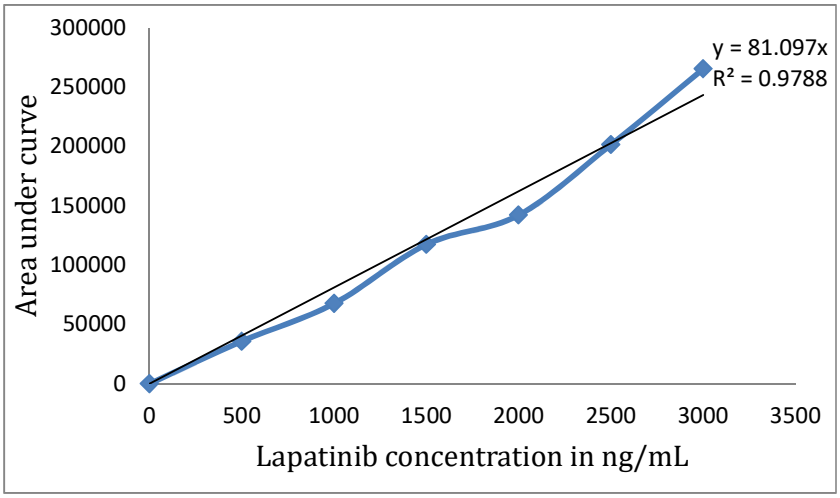

Figure 5.1 Calibration curve of Lapatinib in methanol

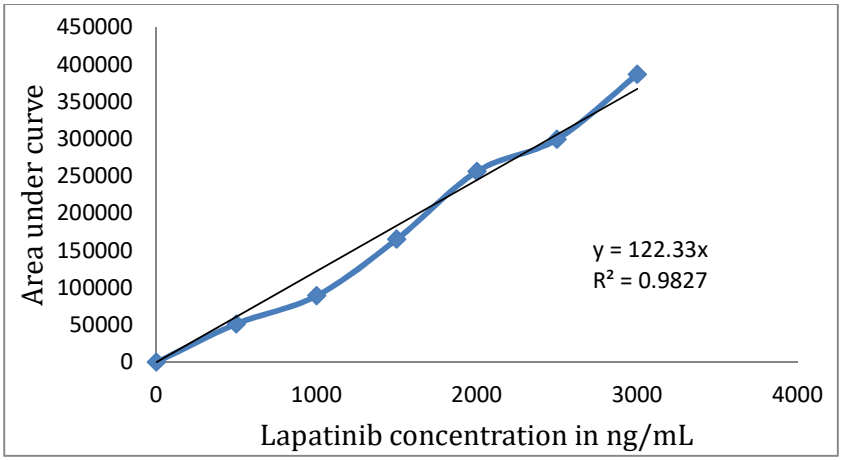

Figure 5.2 Calibration curve of Lapatinib in plasma

5.1.1.1 Range and Linearity

The calibration curves were constructed using six concentrations of LP in the range of 500-3000 ng/ml, and regression parameters like slope and correlation coefficient of these plots were calculated as shown in **Table 5.1**. It was observed that linearity was followed in the analyzed concentration range. The values of correlation coefficients confirmed their suitability for the further analysis.

Table 5.1 HPLC validation parameters for the determination of lapatinib

Parameter	Methanol	Plasma
Wavelength	262	262
R^2	0.973	0.982
Slope	81.09	122.3
LOD (ng/ml)	145	173
LOQ (ng/ml)	440	524
Range (ng/ml)	500-3000	500-3000

5.1.1.2 Accuracy and Precision

Table 5.2 Inter and Intraday accuracy and precision for HPLC analytical method validation

Concentration (ng/ml)	Accuracy		Precision	
In Methanol				
	Intraday	**Inter day**	**Intraday**	**Inter day**
1500	98.11±0.9	98.92±1.64	0.92	1.66
2000	100.69±1.21	99.47±2.01	1.22	2.03
2500	101.13± 1.39	101.18±1.79	1.40	1.91
In plasma				
1500	100.34±2.39	99.28±1.77	2.38	1.79
2000	103.27±1.35	102.26±0.73	1.31	0.72
2500	98.08±0.52	98.13±1.13	0.53	1.15

All data presented as Mean ± SD, n=3.

The parameters were calculated by running 3 different concentrations within the range used for calibration in triplicate and the results are tabulated in **Table 5.2**. The results indicated that the accuracy of the method was in fair agreement between true and experimental values. Similarly, the % RSD values for intra and interday validation for precision were less than 3% revealed the repeatability and intermediate precision of the developed analytical method.

5.1.1.3 Specificity and sensitivity

Specificity of the analytical method was verified by using the sample from prepared dosage form as an analyte. The peak of LP was not interfered by any of the peaks of the excipients confirming the specificity of the developed method. Further, the developed method should be sensitive enough to determine the lower concentration of the drug in the samples. Thus, parameters like LOD (Limit of detection) and LOQ (limit of quantification) were calculated using slope of standard curve and standard deviation (SD) of response; given in **Table 5.1**.

5.1.2 Determination of critical micelle concentration (CMC)

Generally, iodine hydrophobic probe based method is used to determine the CMC. In this method iodine (I_2), as a hydrophobic probe, was employed where its absorbance steeply rises as the amphiphilic polymer self-assemble into micellar shape and the resulting concentration of polymer was considered as the CMC. The absorption intensity versus SOL concentration profile is depicted in **Figure 5.3 (A, B)**. The CMC was calculated from the graph and the point of intersection of two straight lines was considered as CMC. The CMC of SOL was found to be 6.63×10^{-3} mg/mL, which corresponds to the previously reported value of 7.6×10^{-3} mg/mL [Singh et al. 2018, Yu et al. 2013], and higher than reported values of commonly used surfactants such as

Tween® 21 (2.84×10^{-3} mg/mL) [Di Marzio et al. 2011]. However, the blending of another amphiphilic polymer, PF127, resulted in reduction of the CMC value to 4.4×10^{-3} mg/mL for combination of the both, SOL and PF 127, as expected. Similarly, CMC of SHS was decreased to 4.33×10^{-2} mg/mL from 9×10^{-2} mg/mL (reported in literature) [Younes et al. 2018].

Amphiphiles with low CMC values are desired when they are intended to be used for the formulation of drug delivery systems to improve their integrity in body fluids. One of the important characteristics of amphiphilic polymers is CMC that helps in determining the thermodynamic stability (disassembly potential), *in-vitro* and *in-vivo* kinetic stability (disassembly rate) along with the solubilization capacity of PMs. The observed reduction in CMC might be due to the enhanced contributions of hydrophobic portions of the polymers and their augmented interaction with the aqueous environment [Trivedi and Kompella 2010]. Two reported phenomena could clarify the observed decrease in CMC of the combination of polymers. First, surfactant molecules were adsorbed onto the surfaces to lower the surface tension. Further addition of another surfactants resulted into intercalation of molecules with those of first surfactant which further reduced the surface tension. Thus, a smaller amount of mixed surfactant required for reduction in the surface tension below the CMC level and thus micellization phenomena achieved at lower concentrations. The CMC can be lowered owing to the synergistic effect of the two surfactants [Sheng 2013].

Second, several researchers stated that when the chain length of the hydrophobic element, or in other words, the hydrophobic portion, increases, the CMC is lowered [Lu and Park 2013]. The higher proportion of the hydrophobic parts favors the micellar association in order to achieve thermodynamic stability, in which the interaction of the increased hydrophobic portions with the aqueous portion is significantly reduced

[Muherei and Junin 2009, Sheng 2013]. Conclusively, the direct proportion exist between the thermodynamic stability and the hydrophobic chain length/portion and the contribution of the hydrophobic portion of the amphiphile while CMC is inversely proportional to the thermodynamic stability [Batrakova et al. 2006, Lu and Park 2013]. Similar synergistic effects for lowering the CMC by the mixture of surfactants were previously reported for mixture of surfactant and polymer [Nagarajan 2001], for mixture of Tween 80 and Tween 20 [Rehman et al. 2017], and for the combination of SHS and SOL [Bhuptani et al. 2016].

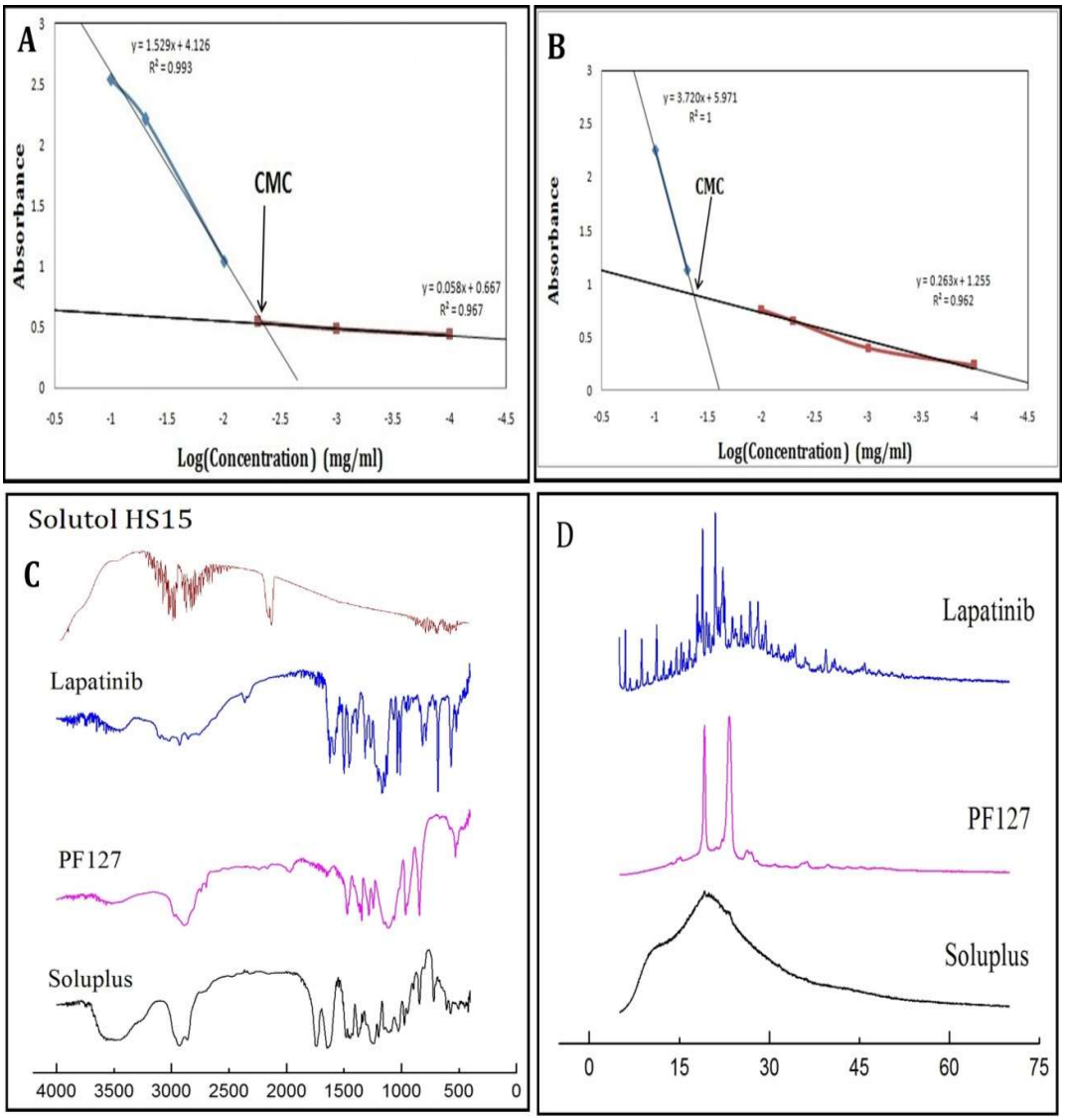

Figure 5.3 Graphs showing CMC determination of combination of (A) SOL and PF127 (B) SOL and SHS; (C) FT-IR spectra and (D) XRPD diffractograms of LP and pharmaceutical excipients

5.1.3 Physicochemical characterization of LP and excipients

5.1.3.1 Fourier Transform Infra-red (FT-IR) study

The FTIR spectra of LP, SOL, PF127, SHS is shown in **Figure 5.3(C).** The characteristic absorption peaks in the spectra of LP are 1147 cm^{-1} (C–F aromatic), 1622 cm^{-1} (C=N stretching), 1313 cm^{-1} (O=S=O), 785 cm^{-1} (C– Cl aromatic), 3065 cm^{-1}

(N–H stretching), with other peaks at 1558 cm^{-1} and 1456 cm^{-1} (C=C aromatic stretching), 2853 cm^{-1} (C–H stretching), 3017and 3065 cm^{-1} (sp^2C–H stretching of aromatic ring), etc. [Mobasseri et al. 2017, Wan et al. 2015b]. The absorption bands of PF127 appeared at 1112 cm^{-1} (C–O stretching), 2883 cm^{-1} (in-plane O–H bending), 1344 cm^{-1} (in-plane O–H bending), and 3524 cm^{-1} (C–H stretching of the aliphatic portion and O–H stretching) [Al Kayal et al. 2015]. The spectra of SOL exhibited absorption bands at 3350–3650 cm^{-1} (intermolecular hydrogen bonded O–H stretching), 2929 cm^{-1} and 2860 cm^{-1} (asymmetric and symmetric aliphatic C–H stretching), 1734 cm^{-1} (carbonyl stretching of $OC(O)CH_3$ of ester); 1481 cm^{-1} (C–O–C stretching), 1446 cm^{-1} (CH_3 bending), 1636 cm^{-1} (carbonyl stretching of C(O)N of amide), 1242 cm^{-1} and 1109 cm^{-1} (C–O stretching of ester), respectively [Lee et al. 2015, Lin et al. 2016]. Moreover, the spectra of SHS exhibited peaks at 2995 cm^{-1}, which may be assigned to C–O stretching [Al Kayal et al. 2015].

5.1.3.2 X-ray Powder Diffraction (XRPD) study

The physical states of SOL, PF127 and LP were determined by XRPD analysis, and **Figure 5.3(D)** depicts their diffractogram. The diffractogram of LP exhibited sharp characteristic peaks at 18.04°, 18.9°, and 21.02° indicating crystalline nature of LP; the data were similar to those recorded in earlier literature [Wan et al. 2015b]. The amorphous nature of SOL was confirmed by a broad halo or absence of a sharp peak in XRPD spectra [Zhang et al. 2016], while diffractogram of PF127 showed the presence of two sharp peaks at 19.22° and 23.36°. The SHS has a waxy semisolid consistency, thus cannot be analysed by XRPD technique.

5.2 Development, optimization and evaluation of Lapatinib-loaded Polymeric Micelles (LP-PMs)

5.2.1 Screening of components for the formulation of micelles

The Quality-by-Design approach was used for optimization of the formulation. For the purpose, a hypothetical quality target product profile (QTPP) was prepared depending on the desired characteristics and the parameters are tabulated in **Table 5.3**. Trough a critical literature review, various parameters those had a potential effect on the product qualities are ensembled to prepare a controlled impact matrix (**Table 5.4**) and the critical process parameters (CPP) and material attributes (CMA) (**Table 5.5**) were identified which were likely to be impacting the characteristics of micellar formulation. Further, risk estimation matrix was constructed depending on the intensity of the influence those CPP and CMA could have on the targeted product.

Table 5.3 Quality Target Product Profile

Attributes	Target	Justification
Dosage form	Micelles	Core-shell structure of micelle can encapsulate the highly hydrophibic drug and reported to improve its bioavailability, nano-carrier systems helps in passively targeting the drug to cancer tumours
Dosage design	Sustained release	Reduction in dose of drug and dosage frequency with reduced dose related toxicity to unintended organs
Finished product	Lyophilized powder	Improved stability
Route of administration	Intravenous	Major portion of drug is remained unabsorbed and excreted via feces due to hydrophobicity of drug. For targeting tumors
Stability	At least 12 months	To maintain the therapeutic potential of the drug.

Table 5.4 Control Impact Matrix

CONTROL	IMPACT		
Critical quality attributes (CQAs)	**High**	**Medium**	**Low**
In Control of formulator	Type of water Selection of organic solvent and its volume used Selection and type of excipients Amount of excipients and LP The ratio of excipients in combination Amount of surfactant Temperature, speed of rotation and vacuum applied during rotary evaporation Method of formulation Volume of hydration solvent Time of hydration	Efficiency of formulator	-
Out of Control	Solubility of drug Purity of excipients Efficiency of analytical systems Environmental conditions (Room temperature, humidity, pressure, etc.)	Efficiency of Formulator, Analyst, Chemist.	Contamin-ation

Table 5.5 Critical process parameters and material attributes

Sr. No	CPPs	CMAs
1.	Method of formulation	Types of excipients used, drug:polymer ratio and solubility of drug
2.	Rotary evaporation	Concentration of excipents and amount of organic solvent
3.	Time for hydration	Co-surfactant used, quantity of hydration solvent
4.	Temperature for evaporation	Type of organic solvent used

Table 5.6 Risk Estimation Matrix

CTQ (CMAS+ CPPs)	Particle Size	Polydispersity Index	Entrapment Efficiency
Types of excipients	High	Low	High
Solubility of drug	Medium	Low	High
Drug:polymer ratio	High	Low	High
Concentration of excipients	High	Low	High
Amount of organic solvent	High	High	Low
Type of co-surfactant used	Medium	Medium	Low
Amount of co-surfactant used	High	High	Low
Quantity of hydration solvent	Medium	Medium	Low
Rotary evaporation	Medium	Low	Medium
Temperature for evaporation	Low	Low	Low
Time for hydration	Medium	High	Low
Temperature for evaporation	Medium	Medium	Low

The PB design was employed by considering 12 factors at 2 levels from risk estimation matrix (**Table 5.6**) for determining the effect on 3 responses, as tabulated in **Table 5.7**. The Pareto charts depicting the factors significantly influencing the selected responses are given in **Figure 5.4**. All the three responses was found to be influenced by type of excipient i.e. polymer, and solvent used for solubilization of drug used during preparation of micelles. These common factors influencing all the three responses were then selected troughs the preliminary experimentation where various polymers were used for preparation of micelles. From our observations, we selected two polymers viz. SOL and PF127, depending upon the size of micelles, for further optimization. Also, the quest of selection of organic solvent was resolved by selecting methanol as a solvent for drug. In addition, the factors influencing PS was amount of polymer used whereas PDI was affected by the amount of organic solvent. The EE was significantly affected by amount of co-surfactant in addition to above-mentioned factors. These three factors

influencing each of the response were then selected for final optimization of formulation.

Table 5.7 Details of factors used for Placket-Burman design

	Independent Variables	Low Level	High Level	Unit	Type of factor
A.	Types of excipients	Pluronic F127	Soluplus®	-	Category
B.	Solvent for drug	DMF	Methanol	-	Category
C.	Time for rotary evaporation	30	60	min	Numeric
D.	Type of co-surfactant used	Pluronic F68	Pluronic F127	-	Category
E.	Speed of rotation during Rotary hydration	20	80	RPM	Numeric
F.	Quantity of hydration solvent	5	15	mL	Numeric
G.	Speed of rotation during evaporation	40	80	RPM	Numeric
H.	Temperature for evaporation	20	40	^{0}C	Numeric
J.	Time for hydration	30	60	min	Numeric
K.	Amount of polymer	75	125	mg	Numeric
L.	Amount of co-surfactant	0	1	% w/v	Numeric
M.	Amount of organic solvent	15	25	mL	Numeric

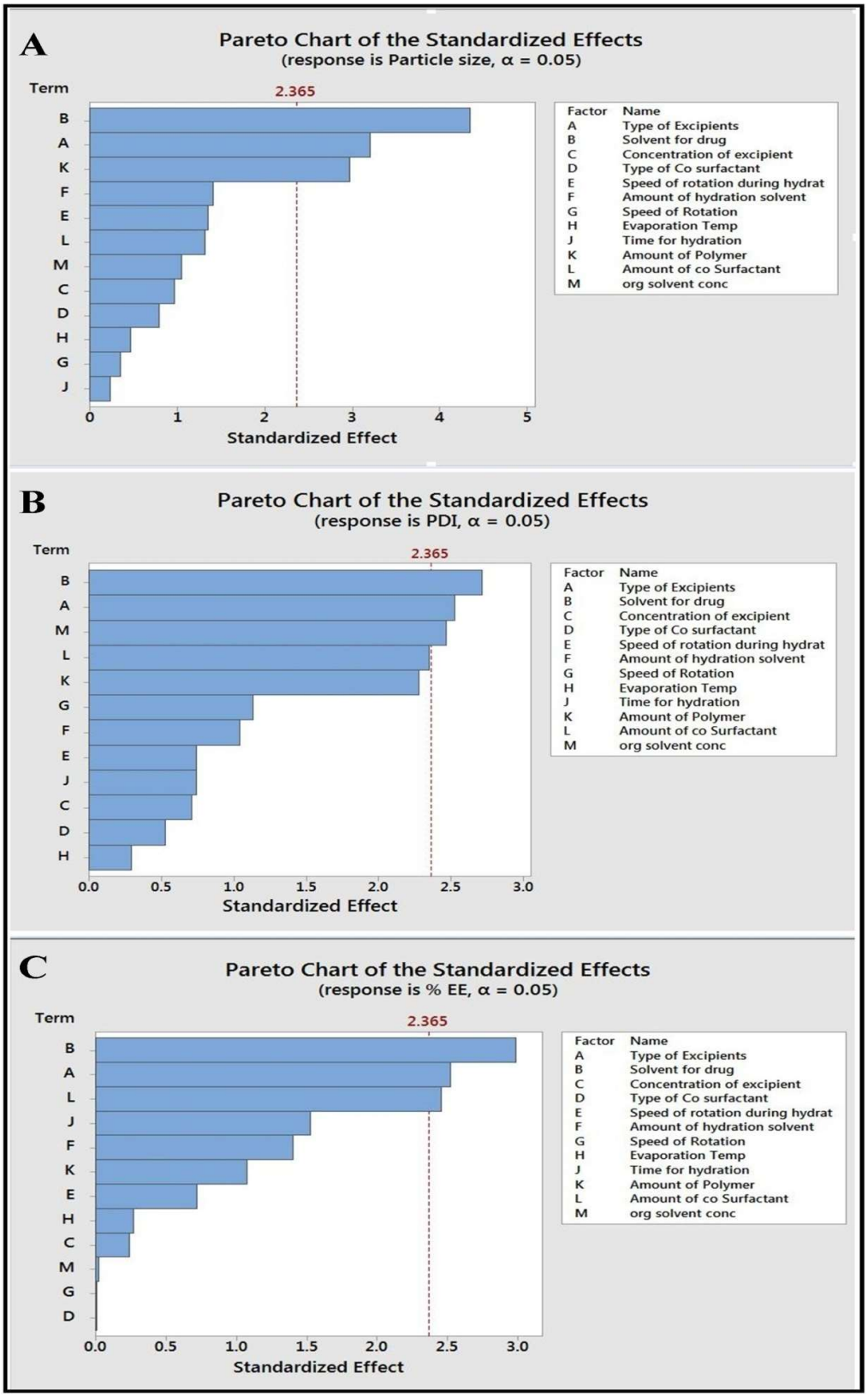

Figure 5.4 Pareto chart showing the influence of process variables on (A) particle size (B) polydispersity index, and (C) entrapment efficiency

5.2.2 Optimization of micelles by Box-Behnken Design (BBD)

The BBD experimental design was used with 3 independent variables at 3 levels having total 17 runs. Design Expert Software was used to estimate the interaction of the independent variables among themselves and their effect on responses. Based on these interactions, the optimized formulation (LP-PMs) was prepared and the levels of independent variables were optimized as per need. The experimental findings for each response are shown in **Table 5.8**.

Table 5.8 Composition of LP-PMs as per BBD design

Batch Code	API:Polymer ratio (w/w)	Methanol (mL)	Co-surfactant (%)	Paticle Size (nm)*	PDI*	EE* (%)	DL* (%)
1	1:5	20	0.5	93.6 ± 3.1	0.099 ± 0.012	84.71 ± 5.73	9.97 ± 0.67
2	1:5	15	1	116.0 ± 2.6	0.292 ± 0.016	82.53 ± 4.75	7.50 ± 0.43
3	1:5	15	0	125.2 ± 2.0	0.304 ± 0.030	72.31 ± 6.72	12.05 ± 1.12
4	1:6.25	25	0.5	72.8 ± 4.9	0.235 ± 0.032	83.82 ± 3.18	8.60 ± 0.33
5	1:3.75	25	0.5	112.3 ± 2.0	0.267 ± 0.004	72.75 ± 9.36	10.03 ± 1.29
6	1:5	20	0.5	94.9 ± 1.5	0.122 ± 0.028	84.79 ± 4.95	9.97 ± 0.58
7	1:3.75	20	1	130.4 ± 1.8	0.261 ± 0.029	71.86 ± 10.31	7.37 ± 1.06
8	1:5	20	0.5	92.9 ± 4.1	0.093 ± 0.018	82.13 ± 4.69	10.76 ± 0.90
9	1:6.25	20	0	108.8 ± 2.3	0.255 ± 0.005	75.81 ± 2.47	10.46 ± 0.34
10	1:5	25	1	97.9 ± 2.9	0.207 ± 0.014	84.02 ± 5.55	7.64 ± 0.51
11	1:3.75	20	0	108.4 ±2.1	0.307 ± 0.022	64.03 ± 12.06	13.48 ± 2.54
12	1:5	20	0.5	95.5 ± 1.2	0.100 ± 0.010	84.05 ± 6.52	9.89 ± 0.77
13	1:5	20	0.5	95.4 ± 1.7	0.097 ± 0.007	86.07 ± 5.39	10.13 ± 0.63
14	1:6.25	20	1	79.9 ± 1.8	0.226 ± 0.007	81.49 ± 4.38	6.65 ± 0.36
15	1:5	25	0	102.6 ± 7.4	0.285 ± 0.062	88.14 ± 3.87	14.69 ± 0.65
16	1:3.75	15	0.5	120.8 ± 2.3	0.288 ± 0.013	71.84 ± 6.93	9.91 ± 0.96
17	1:6.25	15	0.5	112.8 ±2.4	0.265 ± 0.012	79.78 ± 5.98	8.18 ± 0.61

*All the results are mentioned as mean ± standard deviation, n=3.

5.2.2.1 Influence of independent variables on particle size

The average PSs of all the formulated batches of micelles ranged from 72.8±4 nm to 130.4±7 nm (**Table 5.8**). The negative coefficients of the chosen independent variables imply significant ($p<0.05$) negative impact on PSs. The relationship between PSs and

independent variables is well understood by the following polynomial equation:

$$\text{Particle Size} = 94.84 - 11.99A - 11.27B - 2.21C - 7.43AB - 12.70AC + 1.93\,BC + 3.78A^2 + 6.55B^2 + 8.23C^2$$

The Model F-value of 476.63 ($p < 0.05$) suggests the significance of the chosen model. The "Lack of Fit F-value" of 4.16 was insignificant. However, "Predicted R^2" of 0.9796 was in legitimate agreement with the "Adjusted R^2" of 0.9963, which indicates the adequacy of the model.

5.2.2.2 Influence of independent variables on polydispersity index (PDI)

Figure 5.5(C, D) illustrates the effect of the independent variables on PDI which can be further well understood by the following equation:

$$PDI = 0.10 - 0.018A - 0.019B - 0.021C - 2.250AB + 4.250AC - 0.016\,BC + 0.076A^2 + 0.086B^2 + 0.084C^2$$

The average PDI of the micelles ranged from 0.093±0.018 to 0.304±0.030 (**Table 5.8**), and the specified independent variables were found to have a significant effect ($p<0.05$) on PDI. Further, the Model F-value of 79.61 ($p<0.05$) suggests the significance of the chosen model. The "Lack of Fit F-value" of 1.30 was insignificant. The "Predicted R^2" of 0.9158 was in agreement with the "Adjusted R^2" of 0.9779, which indicates the adequacy of the model.

5.2.2.3 Influence of independent variables on encapsulation efficiency (EE)

The average EE of the LP-PMs was ranged from 64.03±12.06% to 88.14±3.88% (**Table 5.8**). The influence of the independent variables on EE is given by the following equation:

$$EE = 93.52 + 5.05A + 2.78B + 2.45C + 0.78AB - 0.54AC - 3.59BC - 12.46A^2 - 4.01B^2 - 7.76C^2$$

The positive coefficients suggested a direct and significant ($p<0.05$) relationship in between the independent variables and EE. Similarly, the Model F-value of 28.55 ($p<0.05$) suggests the significance of the chosen model, whereas the "Lack of Fit F-value" of 2.88 suggests its non-significance. From the three-dimensional (3D) response surface plots [**Figure 5.5(E, F)],** it can be seen that by keeping one variable constant, the other two had optimum effects around the mid-points of the design.

The statistical summary of the ANOVA results are shown in **Table 5.9**. From the statistical analysis of the above experimental findings, LP-PMs were optimised by Design Expert Software, with keeping the PS and PDI minimised while maximising the EE. The LP-PMs constituted a drug:polymer ratio of 1:5.46, 21.78 mL of methanol, and 0.59% PF127, at 0.887 desirability. The prepared LP-PMs were then used for subsequent evaluations and the results are given in **Table 5.10**.

Table 5.9 Statistical ANOVA results of quadratic model generated by Design Expert®

Response	F- value	P-Value*	R^2	R^2 (adj)	CV%	Lack of fit	Remark
PS (nm)	476.63	<0.0001	0.9984	0.9963	0.89	4.16	Significant
EE (%)	28.55	<0.0001	0.9735	0.9394	2.88	2.88	Significant
PDI	79.61	<0.0004	0.9903	0.9779	7.67	1.30	Significant

R^2 (adj) = R^2 adjusted; CV= Coefficient of variation; * statistically significant ($P<0.05$)

Table 5.10 Predicted and experimental values for optimized LP-PMs

Independent variables		**Predicted Levels for optimization**
X_1 **:** API:Polymer ratio (w/w)	-	1**:**5.46
X_2 **:** Methanol (mL)	-	21.78
X_3 **:** Co-surfactant (%)	-	0.59
Dependent variables		**Constraints for optimization**
Y_1 **:** Particle size (nm)	-	Minimum
Y_2 **:** Polydispersity index	-	Minimum
Y_3 **:** Entrapment efficiency (%)	-	Maximum
Desirability of model: 0.887		
Response:	**Predicted values**	**Experimental values***
Particle size (nm)	85.99 nm	92.9 ± 4.07 nm
Polydispersity index	0.108	0.093 ± 0.083
Entrapment efficiency (%)	94.226	87.23% ± 4.85 %

*The results are mentioned as mean ± standard deviation, n=3.

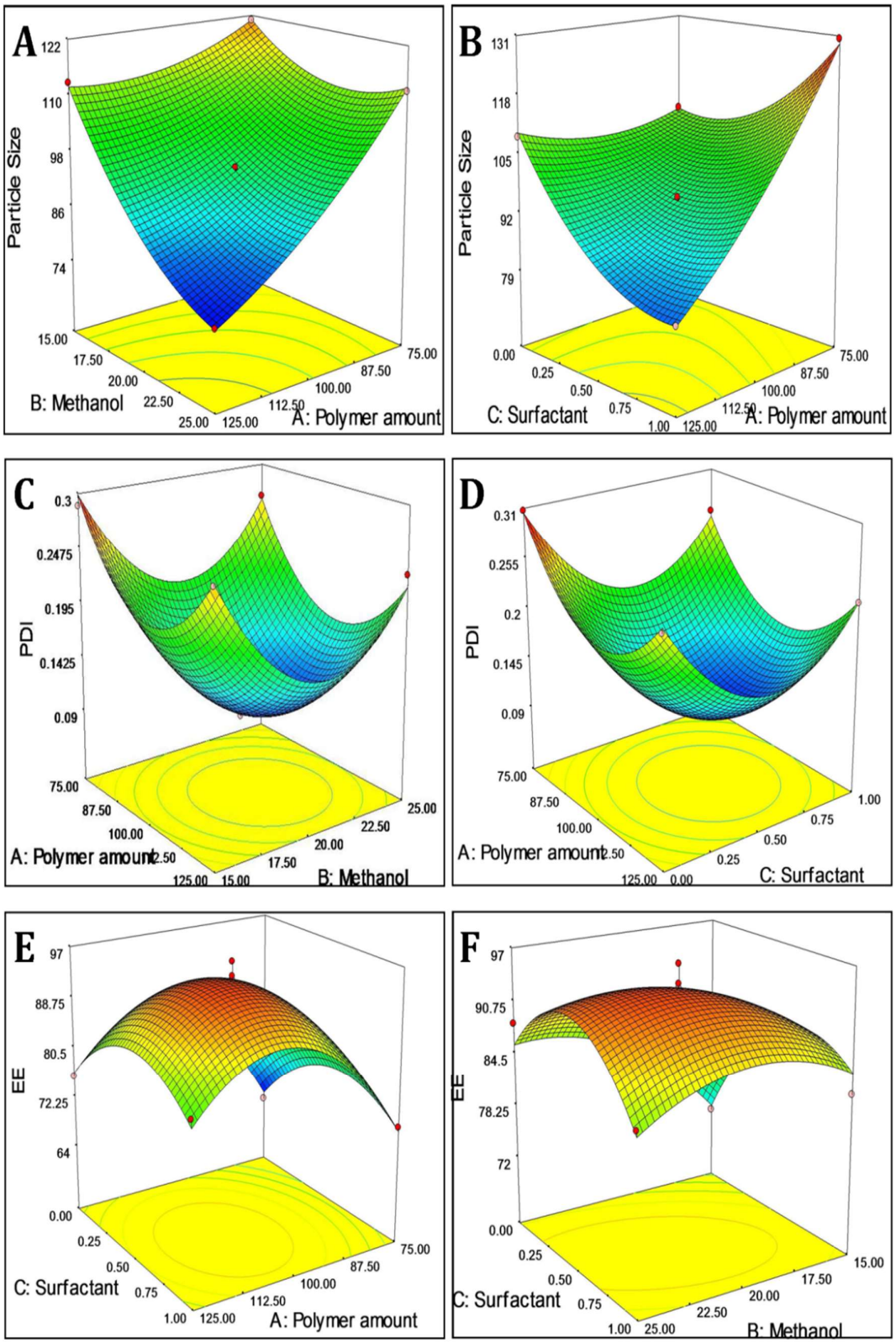

Figure 5.5 3-D response-surface plots showing: (A&B) Effect of independent factors on particle size; (C&D) Effect of independent factors on polydispersity index; and (E&F) Effect of independent factors on encapsulation efficiency

The concept of design of experiment (DoE) trials effectively used for understanding the co-relation between independent and dependent variables, along with the individual and interactive effects of these variables towards the output responses in an organised manner. LP-PMs formulations were optimized based on the BBD design, and 3D response surface plots were derived and are illustrated in **Figure 5.5**. From **Figure 5.5**(A, B), it was observed that the increase in amount of methanol used during preparation resulted in remarkable decrease in mean PS, which might have been due to the formation of a more uniform film during drying and the film formation phase by rotary evaporation. However, the surfactant had an optimum effect around the midpoint, which can be better understood by the fact that the surfactants reduced the surface tension resulting in reduction of PS, but a further increase in PS beyond the mid-point may have been due to the incorporation and aggregation of excess surfactant molecules over the surface of the already prepared micelles.

Further, upon increase in the amount of methanol and surfactant, the initial reduction in the PDI might be due to the uniform film formation during the solvent evaporation as depicted in **Figure 5.5 (C and D).** The presence of optimum surfactant diminished the surface tension, leading to the uniform hydration of the thin film and PMs having similar sizes and smaller PS distribution were formed. Conversely, high content of polymer or surfactant had influenced the hydration phase; therefore, PMs having wide particle size ranges were prepared, resulting in high PDI values. Thus, it could be concluded that for the formulation of nanocolloids (PMs) with uniform size, optimum amount of the polymer and the surfactants need to be chosen carefully.

5.2.3 Formulation of micelles

Various methods such as dialysis method, direct dissolution method, thin-film hydration technique (solvent evaporation method), film sonication method, etc. had been used for preparing PMs by various research groups. The physicochemical properties of the drug and excipients limit the selection of a suitable method for the preparation of PM. In the current research, thin-film hydration method was used for preparation of micelles.

5.2.4 Physicochemical characterization of optimized LP-PMs

5.2.4.1 Particle size and polydispersity index analysis

The prepared LP-PMs were well dispersed in aqueous medium, which was then evaluated for their hydrodynamic diameter and PDI by using DLS technique, and the results are shown in **Table 5.10**. The hydrodynamic diameter of the optimized LP-PMs was found to be 92.9±4.07 nm (8.04% bias) with a PDI of 0.093±0.083 as seen from **Figure 5.6(A).** These results were in accordance with the values the quadratic model predicts. Successful formulation of monodispersed and uniform-sized micelles was indicated by their lower PDI values. Further, the comparison of placebo micelles and lapatinib loaded polymeric micelles demonstrated that size of micelles increased from 57.2 nm to 95.2 nm after loading the LP [**Figure 5.6 (A and B)].** However, the optimum size of drug loaded PMs (less than 100 nm) were thought to have excellent probability for passively targeting the tumors by the EPR effect. The conclusion drawn was based on the reported fact that micelles having size less than 200 nm are better at passive tumor targeting by EPR effect [Huo et al. 2015].

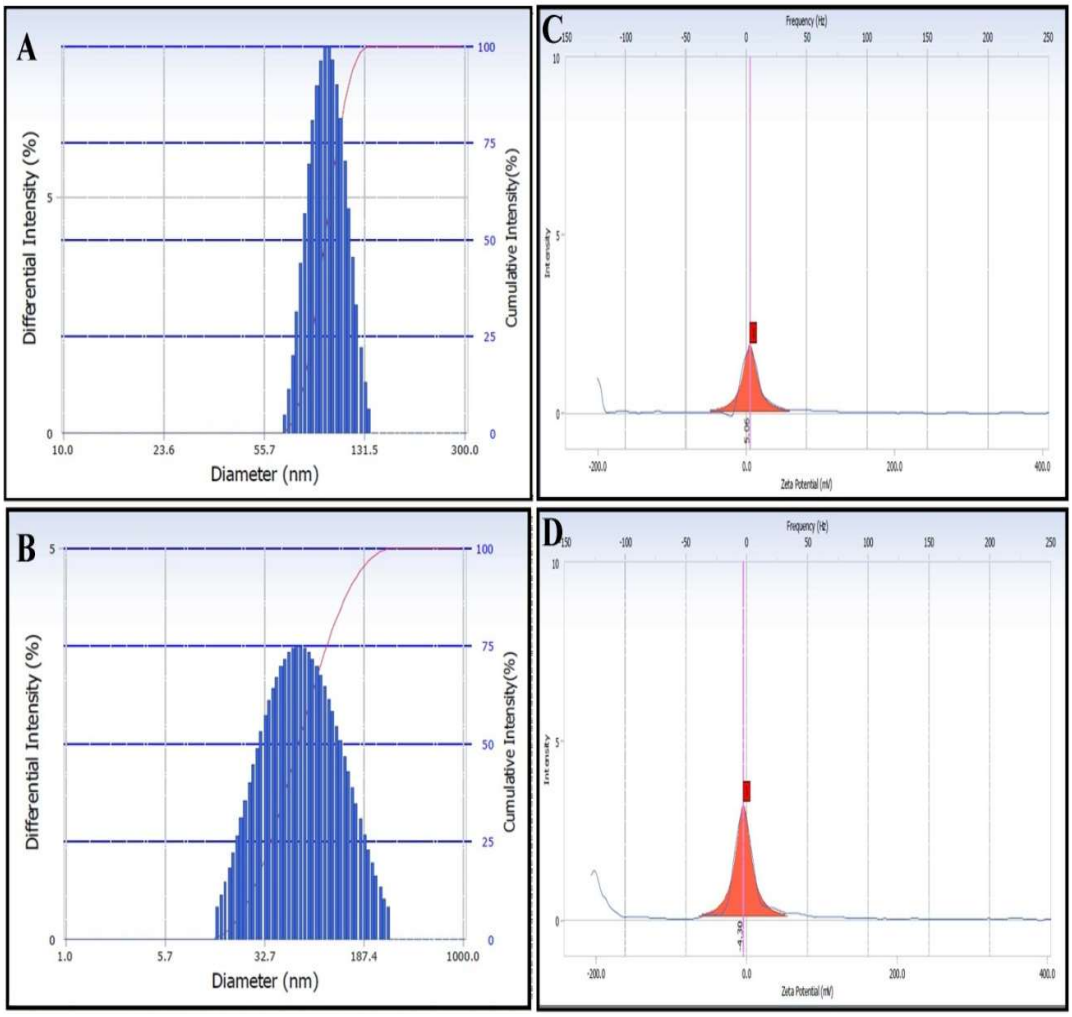

Figure 5.6 Morphological characterization of LP-PMs: Histograms (A and B) and zeta potential (C and D)

5.2.4.2 Zeta potential

Zeta potential of delivery systems depends on the functional groups present in the structure of contributing polymers used for their preparation. The zeta potentials of the optimized LP-PMs and placebo micelles were 5.06 mV and -4.84mV, respectively, depicted from **Figure 5.6(C and D).**

The SOL and PF127 both have hydrophilic PEG, having –OH functional groups. These moieties provided a negative zeta potential to blank micelles in aqueous environment [Jin et al. 2015]. The intermolecular hydrogen bonding between LP and excipients

having free –OH was confirmed by FT-IR studies. The contribution in hydrogen bonding might have resulted in the reduction in number of free –OH groups, that contributed to negative zeta potential of blank micelles. In addition, LP has been reported to partially neutralize negative charges on micelles surfaces [Wei et al. 2015a]. The above-mentioned facts may support the observed positive zeta potential of LP-PMs.

5.2.4.3 High Resolution-Scanning Electron Microscopy

The morphology of optimized PMs were observed by using high-resolution scanning electron microscopy (HR-SEM) [**Figure 5.7(A and B)]** which revealed the spherical shape of the micelles. The diameter of the LP-PMs ranged between 62–95, with an average diameter of 81.85±12.44 nm whereas lyophilized LP-PMs exhibited PS of 62.76±14.86 nm. The observed particle size of LP-PMs was slightly reduced than the observation of the DLS studies. This effect was attributed to the form of SOL during study i.e., during HR-SEM sample preparation, micelle got shrinked during drying in sample preparation while DLS takes into consideration the hydrodynamic diameter in the aqueous dispersion of the micelles with their extended hydrophilic PEG chains into the aqueous dispersion medium [Chen et al. 2016].

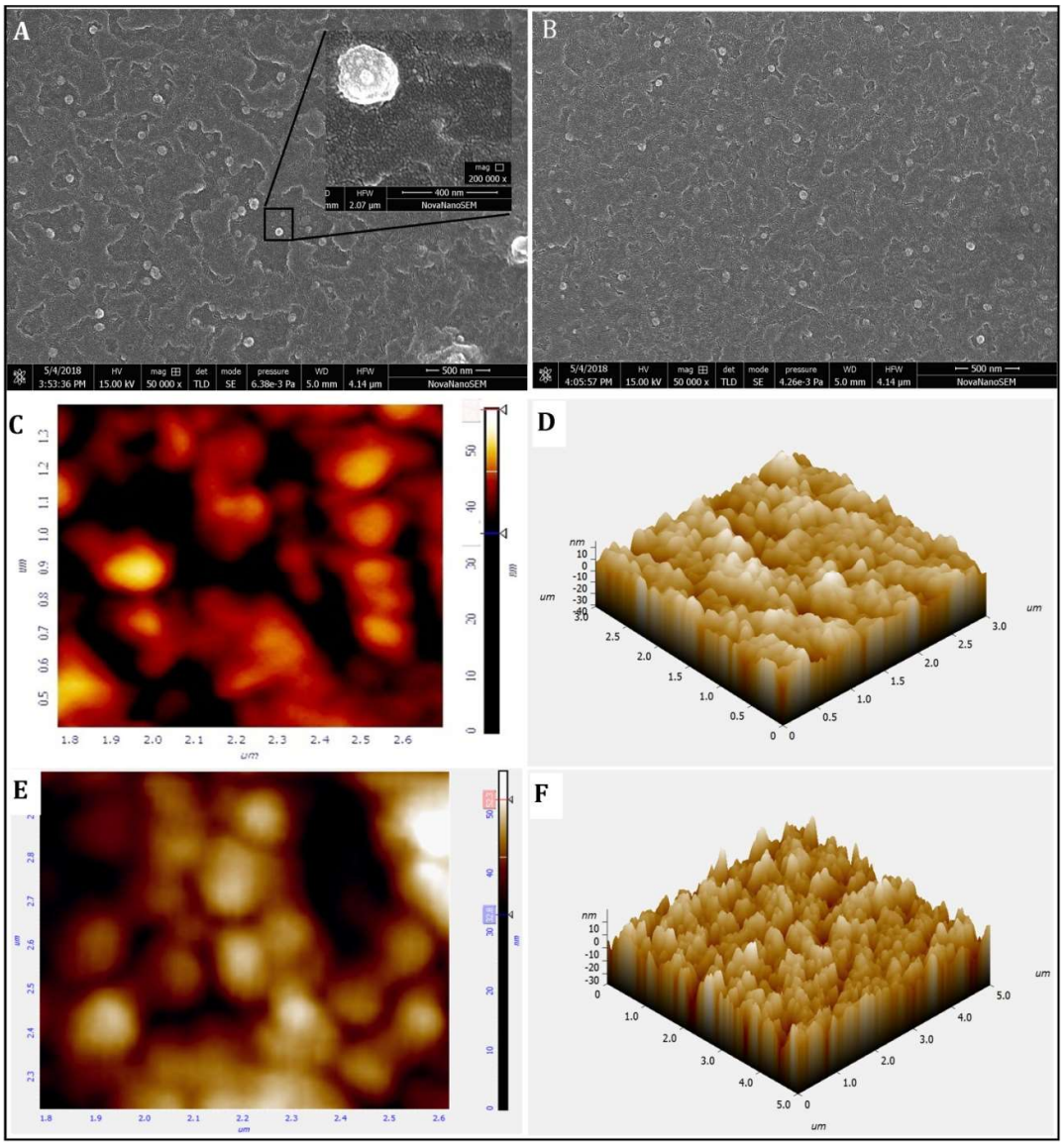

Figure 5.7 Morphological characterization of LP-PMs: High resolution-scanning electron microscopic images (A and B) of LP-PMs and lyophilized LP-PMs, respectively; Scanning probe microscopic images (C and E) and their histograms (D and F) of LP-PMs and lyophilized LP-PMs, respectively.

5.2.4.4 Scanning Probe Microscopy

The SPM technique was used to measure the roughness of the polymeric micelle's surface, and the micelles were found to be spherical in shape, as shown in **Figure 5.7(C and D)**. The average peak-to-peak height of the PMs was found to be 65 nm, which was almost similar to the apparent diameter of the PMs. These findings were in good

agreement with those of the HR-SEM studies.

The SPM images of lyophilized LP-PMs revealed smooth surface with spherical shape of micelles. **Figure 5.7(E and F)** demonstrated that an average peak-to-peak height of 60 nm which may be co-related to apparent diameter of micelle. However, the size visualized by AFM was smaller than that found by DLS in our previous studies. The observed difference was attributed to the drying of PMs during spin coating sample preparation for SPM [Chen et al. 2016].

Nano-delivery systems having size below 200 nm were generally reported to facilitate the passive targeting to the tumors by filtering nanocarriers from blood stream and restraining them to tumors by EPR effect [Huo et al. 2015]. Thus, from the results of morphological evaluations like DLS, HR-SEM and SPM, the prepared LP-PMs were anticipated to have better tumor targeting capability as their size was well below 100 nm. Their spherical shape and smooth surface, characterized by SPM, may facilitate their transit through blood stream and could minimize opsonization and adsorption to the proteins.

5.2.4.5 Fourier Transform Infra-red (FT-IR) study

The FT-IR analysis was performed for determining the compatibility of pharmaceutical excipients and their interactions with drug. The characteristics peaks of polymers and LP were retained in the FT-IR spectra of the physical mixture and drug loaded PMs. However, the broadening of the band around the 3350 cm^{-1} in spectra of drug loaded PMs [**Figure 5.8(A)]** than other individual spectra may suggest intermolecular hydrogen bonding between the LP and SOL [Knop et al. 2011, Yamashita and Takatsuka 2007], which further explain the reason behind the increased solubility and encapsulation of the laptinib in the presence of SOL.

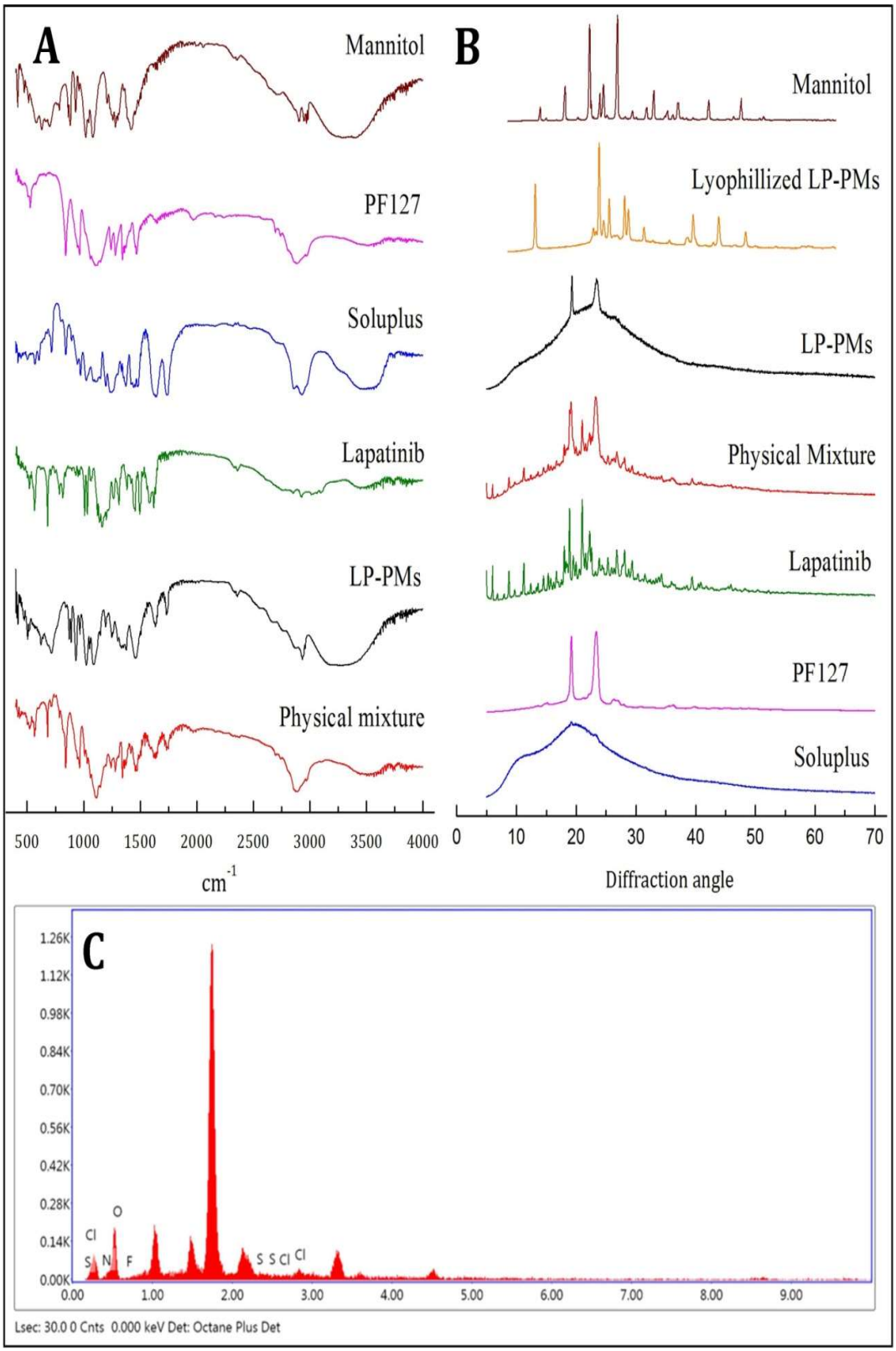

Figure 5.8 (A) FT-IR spectra and (B) XRPD diffractograms of pharmaceutical excipients, LP-PMs (C) EDX spectra of LP-PMs

5.2.4.6 X-ray Powder Diffraction (XRPD) study:

To determine the change in crystallinity of drugs encapsulated into PMs, XRD spectra of pure drugs and polymer were recorded (**Figure 5.8(B)).** The XRPD pattern of the physical mixture revealed a mere superimposition of the three diffractograms of pure drug, SOL, PF127 with reduction in intensity, showing the presence of crystalline LP and PF127 in the physical mixture. However, the LP-PMs revealed a broad halo analogous to SOL and with two superimposed peaks (19.32° and 23.4°) analogous to PF127 without any typical diffraction peaks of LP. Lyophilized LP-PMs showed rather mere addition of some peaks of mannitol (used as cryoprotectant) to the diffractogram of LP-PMs.

Thus, the XRPD study confirmed that LP was successfully encapsulated within the PMs in the amorphous form. The XRPD spectra of LP-PMs was similar to those of SOL and PF127, thus confirming that the outer shell is made up of SOL with a sheath of PF127 over the micelle. Therefore, the experimental findings confirmed that existence of core–shell structure of micelles incorporating the drug within the polymeric shell [Wei et al. 2015a].

5.2.4.7 Energy dispersive X-ray Analysis (EDX)

The optimized micelles were subjected to EDX analysis to verify the elements present in micelle. As depicted from **Figure 5.8(C)**, EDX spectra of LP-PMs showed the presence of carbon, hydrogen and oxygen with fluorine and sulfur that are typical constituents of LP and absent in SOL and PF127 molecules. The results indicated not only the successful encapsulation of drug inside micelle but also some of the drug was also present on the surface of the LP-PMs. Conclusively, the presence of fluorine and sulfur in EDX spectra, and disappearance of peaks of LP in XRPD of formulation confirmed successful incorporation of LP in amorphous form in LP-PMs.

5.2.4.8 Effect of dilution

The observed particles size of the original micelles gradually decreased from 126.47±5.28 nm to 121.67±9.07, 107.47±7.25, 93.03±10.18 to 56.60±7.69 nm upon dilution with water to 10, 100, 200, and 400 folds, respectively, w. Further dilution upto 500 times leads to micellar dissociation into monomer, since the data could not be recorded by the DLS.

The stability against instant dilution of the LP-PMs was confirmed by diluting them with deionised water. The experimental findings confirmed the maintenance of micellar assembly even upon 400-fold dilution; however, the size of LP-PMs was continued to reduce with increasing dilution. Further dilution beyond 400-fold, the amphiphile concentration might had lowered below the CMC value, which resulted in the dissociation of the micellar assembly completely. The observed reduction in the size can be justified on the basis of well-known fact that the dynamic equilibrium existed between the component amphiphilic polymer molecules of micelles and the free molecules in the bulk of dispersion. The concentration of the amphiphiles in bulk may be maintained by drawing few amphiphiles from micellar assembly that existed before dilution, which may be the reason for the reduction of PS upon dilution. Some previous reports from the literature also resembled the observed findings [Bernabeu et al. 2016, Zhao et al. 2017]. Based on results of CMC determination and dilution effect studies, combination of SOL with PF127 indicated the higher kinetic and thermodynamic stability of prepared LP-PMs, which ensures the maintenance of integrity and resistivity of the LP-PMs towards larger extent of dilution in the biological fluids, alleviating the burst release during post-oral/intravenous administration [Oerlemans et al. 2010].

5.2.5 *In-vitro* Evaluations

5.2.5.1 Entrapment Efficiency and Drug Loading

The drug carrying capacity and the suitability of dosage form to deliver the drug at intended site in significant amount is measured by EE and DL. Thus, it becomes crucial to maximize the entrapment efficiency and loading efficiency of drugs into the carriers for utilizing its full potential. Higher loading and entrapment efficiency ensure that more amount of drug is available to the target site thus, reducing the overall dose required and side effects associated with it. The PMs consist of a hydrophobic core which supports the loading of water-insoluble drugs such as LP, thereby, increasing the EE and DL of LP in PMs.

The EE and DL of LP-PMs were found to be 87.23% ± 4.85% (-7.428% bias from the predicted value) and 9.27% ± 0.52%, respectively. Lyophilized LP-PMs had displayed entrapment of LP to a little lower extent as EE and DL of the formulation were found to be 85.23 ± 8.57 % and 2.48 ± 0.25%, respectively. The high EE is due to the hydrophobic core of SOL micelles which interacts suitably with LP (hydrophobic drug) and the findings are in good agreement with the previously reported works [You et al. 2007]. However, the free LP tends to form intermolecular hydrogen bonds with excess SOL (confirmed by FT-IR studies) in an aqueous environment. This is responsible for the solubilisation of LP to some extent. Thus, by formulating LP-PMs, greater availability of the drug at target site is ensured along with reduction in the required dose and high dose associated side-effects of the drug.

5.2.5.2 Drug release studies

In-vitro release study of the LP-PMs was carried out using the dialysis bag method. Tween® 80 (0.5%) was added to the release media in order to maintain sink condition. The LP so released from the formulation was quantified using a UV-spectrophotometer.

The cumulative percent release was calculated and the release profile was plotted between %CPR and time. The drug release pattern was influenced by pH and the same has been shown in **Figure 5.9(A).** Around 29% of LP was released towards the end of 24h at pH 7.4. The drug release slowed down later on, with just 36% cumulative drug release for the next 24h. However, at pH 5.0, the LP release was much faster and drug release % was found to be 45% and 60% at the end of 24h and 48h, respectively. Different kinetic models were applied to the data so obtained from the release studies and it was found that the LP release from PMs followed the Higuchi model. The value of the Peppas exponent *n* was found to be 0.477, suggesting that the LP release followed Fick's diffusion.

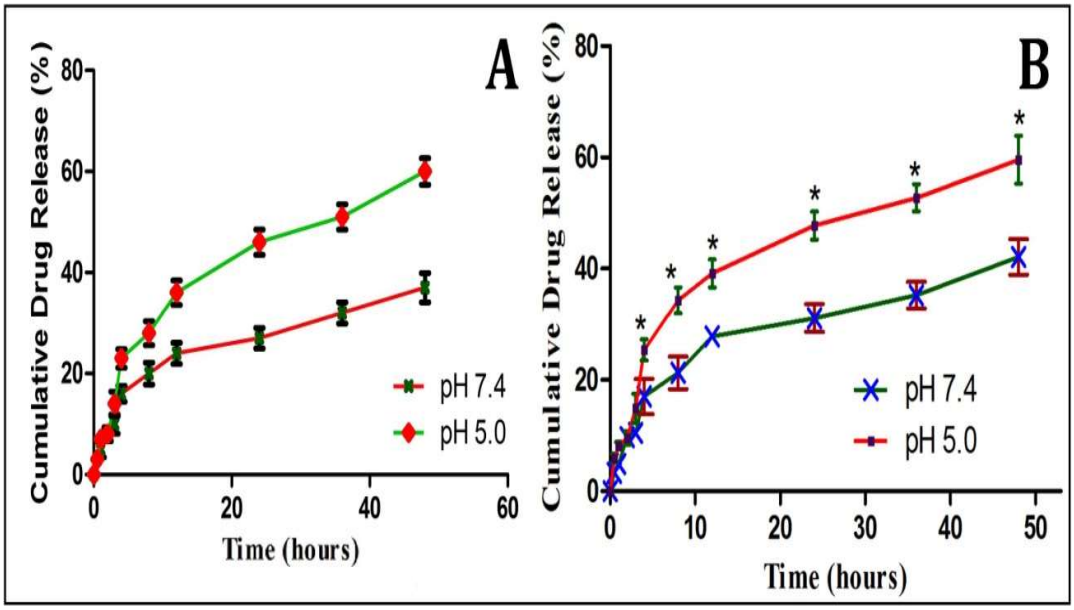

Figure 5.9 *In-vitro* drug release profile of (A) LP-PMs micellar dispersion and (B) lyophillized LP-PMs in release media of pH 5.0 and pH 7.4

From **Figure 5.9(B),** biphasic drug release was witnessed in case of lyophilised LP-PMs, in resepctive of the pH of release medium. The drug release was faster in first phase (for around 12h) which slowed down during the later stage. At pH 5.0, the total LP release was found to be around 49% and 64% at the end of 24h and 48h, respectively

while at pH 7.4, nearly 31% of LP had been released in first 24h and 42% of drug was released during next 24 h. Different kinetic models were applied to the data so obtained from the release studies and it was found that the LP release from PMs followed the Higuchi model. The value of Peppas exponent 'n' was found to be 0.416 and 0.381 at pH 7.4 and pH 5.0, respectively.

The *in-vitro* drug release pattern of the formulation was studied at two different pH conditions simulating the different biological sites through which the formulation was expected to come in contact with. The selected media was pH 7.4 and pH 5.0, which is the pH of the blood and the tumour environment, respectively. Biphasic drug release was witnessed. High rate of drug release was seen in the first few hours of the release study which might be due to faster dissolution of LP which was either present in the bulk of LP-PMs or bound to the surface of LP-PMs. During the initial period, the rate of drug release from same formulation at two different pH were similar, while a significant difference ($p<0.001$) in cumulative drug release was witnessed after 4h. The drug release slowed down during the second stage which is characterized by flattening of the curve of release profile wherein the entrapped drug was slowly released from the micellar structure. The drug release rate from the formulations was higher at pH 5.0 compared to pH 7.4. Later on, by applying different kinetic models, it was found that LP release from formulation had followed the Higuchi model.

The LP-PMs were formulated for delivering the drug specifically to the tumor site. The higher release rate so observed at acidic pH (5.0) might be due to weakening and distortion of hydrogen bonding between LP and SOL resulting in faster release of drug from micelles. The lower release rate at pH 7.4 is also beneficial because this indicates that the drug loss during transit in the blood is minimal thus, avoiding premature release of loaded drug and its associated side effects. The micellar association was found to maintain their integrity and resisted dissociation upon small dilutions in the bulk of

body fluids which was responsible for the prolongation of drug release [Batrakova et al. 2006, Lombardo et al. 2015].

In conclusion, the obtained results suggest that the LP-PMs so formulated can be employed as sustained release drug delivery systems for the delivery of poorly water-soluble drugs that can selectively deliver the drug to an acidic environment of tumor.

5.2.5.3 Haemocompatibility study

The extent of hemolysis caused by LP-PMs or LP only was insignificant with % hemolysis being <1%. However, the comparison of hemolysis caused by LP only and LP-PMs revealed that the drug when in formulation (LP-PMs) caused significantly lower hemolysis ($p<0.01$) as compared to the LP-only group [**Figure 5.10(A)**].

The prepared formulation is required not to cause hemolysis, because the proposed route of administration is I.V. route. Hence, blood which the first major component of the body to come in contact with the formulation, should not be disrupted. Thus, the acceptance of formulation by the blood was evaluated by checking the *in-vitro* hemolysis caused by formulation as well as platelet aggregation after treatment with LP-PMs. Incompatibility of formulation with blood components may either cause thrombosis or lead to RBC hemolysis, increasing risk to the patient in both the cases [Mittal et al. 2019]. Induced hemolysis of less than 1% upon I.V. administration is considered safe for patients [Ajmal et al. 2019]. Our findings confirmed the hemocompatibility of LP-PMs because significantly lower hemolysis ($p<0.01$) was witnessed in the LP-PMs than in the LP-alone group and is attributed to encapsulation of LP inside the micelle.

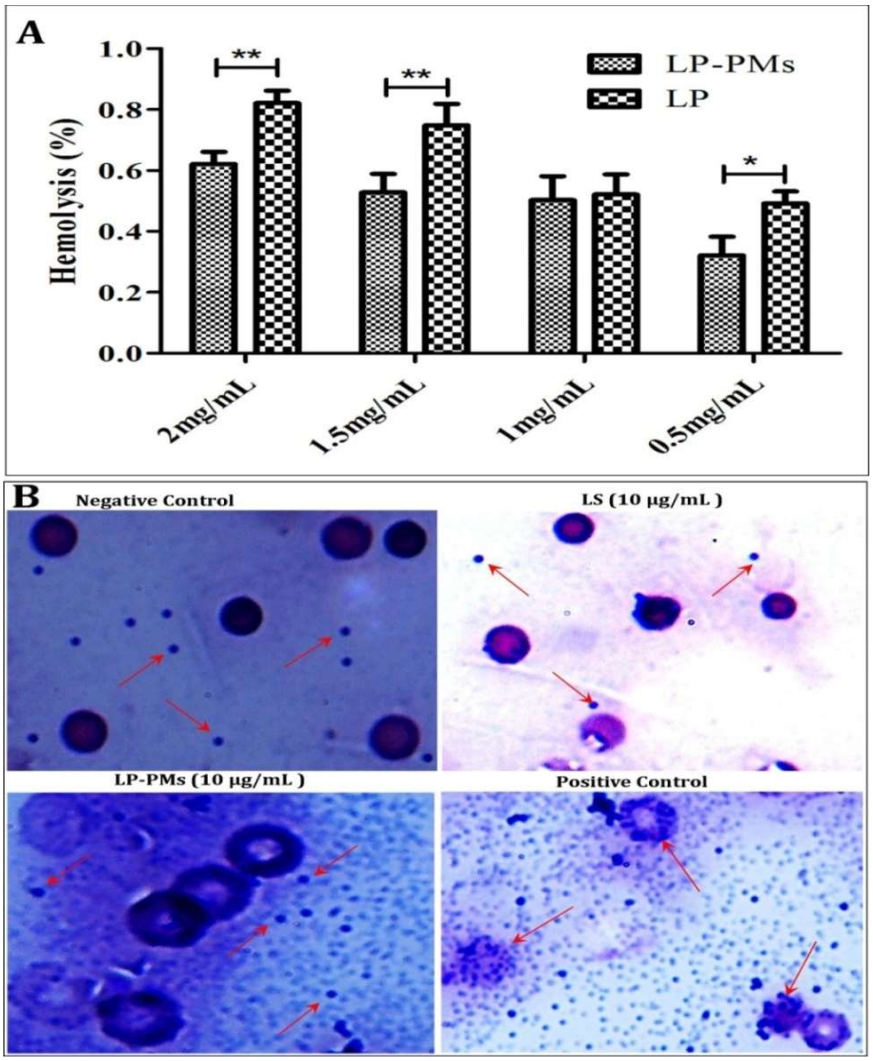

Figure 5.10 Hemocompatibility studies where, (A) represents the percent hemolysis induced by various concentration of lapatinib solution and LP-PMs and (B) reveals no platelet aggregation post-treatment with LP-PMs (* represents $p < 0.05$ and ** represents $p < 0.01$ significant difference)

5.2.5.4 Platelet aggregation studies

Platelet aggregation study was conducted as discussed before and the results shown in **Figure 5.10(B)** which revealed that the platelet morphology was retained and were dispersed discretely all over the slide. Platelet aggregation was not seen either in the control or in the LP-PM–treated blood specimens indicating the good hemocompatibility of the formulation [Mittal et al. 2019]. However, in positive control, the platelets were aggregated on the surface of RBCs. The results from

hemocompatibility studies indicate that the encapsulation of drug inside the PMs decreases the hemolytic capability of LP and makes it safe for I.V. administration.

5.2.6 Stability Studies

Stability studies of the prepared LP-PMs were carried out by storing the formulations at different environmental conditions (temperature and relative humidity) and the effect of these two parameters on the formulation was assessed. The EE of the samples were analysed at each sampling point and no significant changes ($p<0.05$) were found in the LP-PMs which were stored at 5±3°C. However, the formulation stored at 30±2°C/65±5% RH, had shown significant changes within 3 months of the storage period. Thus, these LP-PM batches were withdrawn from the study protocol. The results of EE prior and after the sampling period are shown in **Table 5.11**. Further, the shelf life of the formulation was estimated from EE by using Minitab® version 7, which was found to be 12 months, as shown in **Figure 5.11 (A)**.

Table 5.11 Results of evaluations for stability studies

	Conditions	**30°C ± 2°C/65% RH ± 5% RH**	**5°C ± 3°C**
	Time (month)	**EE (%)**	**EE (%)**
LP-PMs	0	87.23 ± 4.85	87.23 ± 4.85
	3	81.11 ± 8.02	85.04 ± 3.32
	6	Discontinued due to aggregation	82.86 ± 3.94
Estimated Shelf-life (months)		-	12
Lyophilized LP-PMs	0	85.22 ± 8.57	85.22 ± 8.57
	3	83.59 ± 7.80	84.13 ± 8.57
	6	81.77 ± 8.40	82.86 ± 8.15
Estimated Shelf-life (months)		11	15

*All the results are mentioned as mean ± standard deviation, n=3.

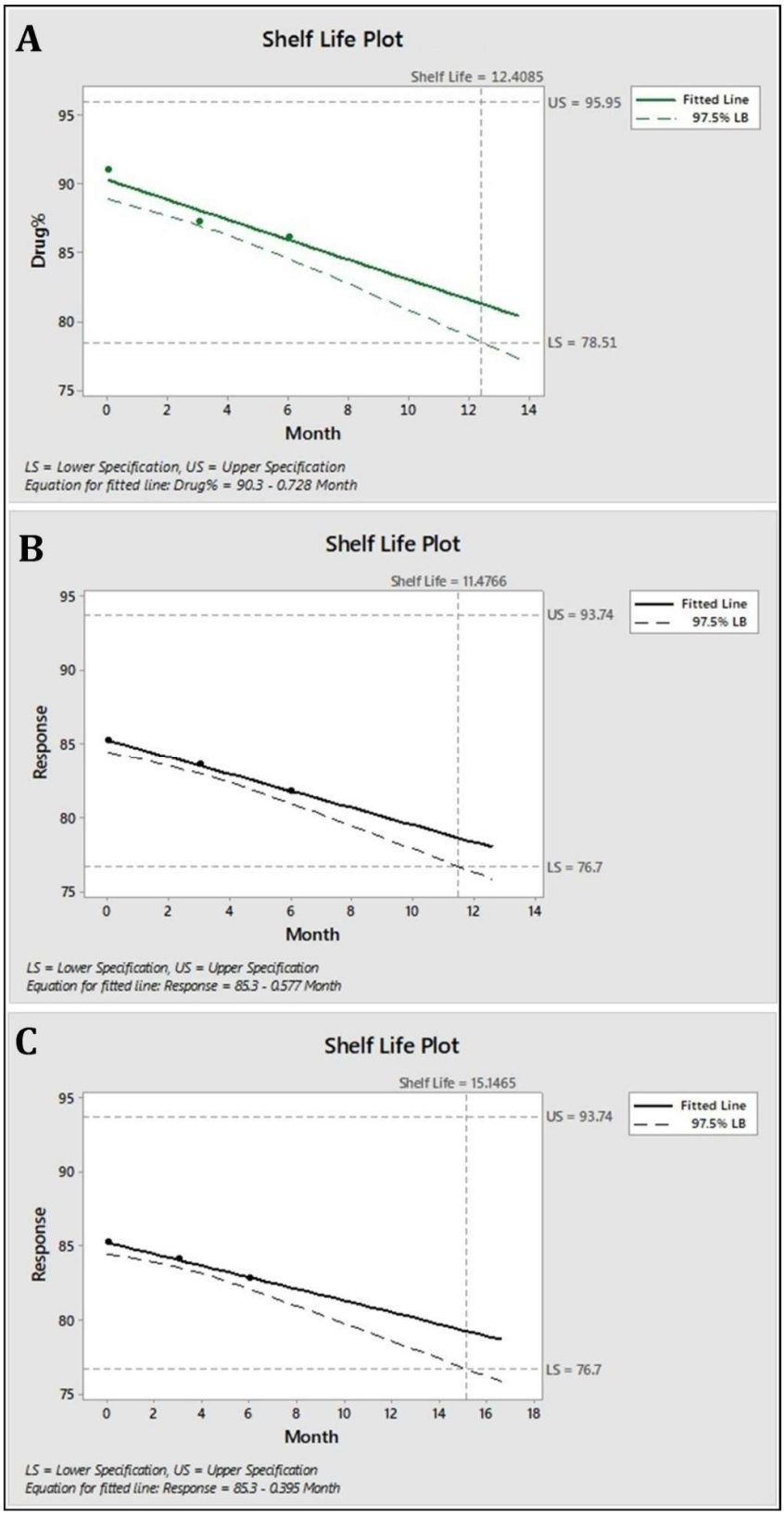

Figure 5.11 Shelf life plots of LP-PMs: (A) in dispersion form at 5°C ± 3°C; (B) in lyophillized form at 30°C ± 2°C/65% RH ± 5% RH; (C) in lyophilized form at 5°C ± 3°C)

In case of lyophilized PMs, non-significant changes ($p<0.05$) were observed when stored at both the conditions as shown in **Table 5.11**. The estimated shelf life was found to be 11 and 15 months at room and refrigerated temperature, as shown in **Figure 5.11(B and C)**, respectively. Marked improvement in stability was seen at 30°C ± 2°C/65% RH ± 5% RH, in comparison to LP-PMs dispersion.

Stability studies were performed to estimate the effects of environmental conditions on LP-PMs and to recommend desirable conditions for its storage. Based on EE observations, it was deduced that the refrigerated conditions should be recommended for the storage of LP-PMs dispersion. Moreover, the results of lyophilized LP-PMs corroborated that the lyophilization resulted in transformation of liquid dispersion to solid powder form that markedly enhanced its stability especially at 30°C ± 2°C/65% RH ± 5% RH, as compared LP-PMs in dispersion form which were aggregated after 3 months. Conclusively, it can be said that the lyophilized LP-PMs are stable even at room temperature, unlike the non-lyophilsied LP-PMs and their stability was further remarkably enhanced at refrigerated temperature.

5.2.7 *In-vitro* screening of anticancer efficacy

5.2.7.1 Cell Culture

In-vitro evaluation of the anticancer efficacy was carried out using SKBr3 breast cancer cell line because of its characteristic feature/ability to over express HER2 [Greenshields et al. 2019, Jeong et al. 2015] and can serve as best for the present study.

5.2.7.2 Cytotoxicity assay

Percent cell viability after treatment with various concentrations of LS and LP-PMs is graphically illustrated in **Figure 5.12(A).** LP-PMs (IC_{50}: 1.60 µg/ml) and had shown better anticancer efficacy over LP only (IC_{50}- 8.19 µg /ml). The results indicated that the

LP-PMs possessed better anti-cancer activity than the free drug against the cell lines.

LP causes the arrest in growth of tumor cell lines that express EGFR and HER2. It binds reversibly to the ATP-binding site of the kinase domain of EGFR and HER2 to prevent autophosphorylation. Thus, LP exhibits antagonistic activity against EGFR and HER2. The cell toxicity/anti-cancer activity of the formulation was evaluated by the MTT-based assay on SKBr3 breast cancer cell line. The activity is being measured in terms of IC_{50} value which represents the concentration of a drug required to inhibition of cell growth by 50% in comparison to controls.

MTT assay results suggested that LP-PMs inhibits the HER2 expressing cancer cell lines as the IC_{50} values of LP-PMs against SKBr3 cell line were significantly lower compared to LS treated SKBr3 cell line. The IC_{50} of LP-PMs was lower by almost 6 folds against SKBr3 in comparison to LS, which indicated the greater anti-cancer efficacy of LP-PMs. Therefore, from the results, it can be concluded that the LP in PMs could potentiate its anti-cancer efficacy [Wan et al. 2015b].

5.2.7.3 In-vitro anti-cancer efficacy studies

Figure 5.12(B) shows morphological changes in SKBr3. The SKBr3 cells are cuboidal and polygonal in shape which is their natural morphology as seen in the field of vision (FOV). The cell morphology after treatment with LP-PMs changed to rounded and the size also shrunk (#), with increased granular cytoplasm content ($), and loss of confluence (*) in the FOV. In LS-treated cultures, only a small percentage of cells had exhibited altered morphology but majority of the cells had retained their original shape.

In order to confirm the anti-cancer efficacy of LP which was encapsulated inside the PMs, the morphological changes in the cells caused by treatment with LP and LP-PMs was estimated. In the LP-PMs-treated cultures, the cytoplasmic condensation was

witnessed which caused the cells to shrink and adopt a rounded morphology. Thus, it can be said that LP-PMs induced apoptosis in the cancer cells [Buttacavoli et al. 2018, Cancemi et al. 2017]. The reason for appearance of granular structure can be due to chromatin shrinking or fragmentation of the nucleus [D'Suze et al. 2010]. The morphological changes and decrease in the number of viable cells in the LP-PMs-treated culture indicate that our findings are in good agreement with those of previous reports. The decreased activity of LS groups can be due to low solubility which results in lower cellular uptake and subsequent decrease in the anti-cancer activity.The placebo micelles had not shown any activity against the SKBr3 cells.

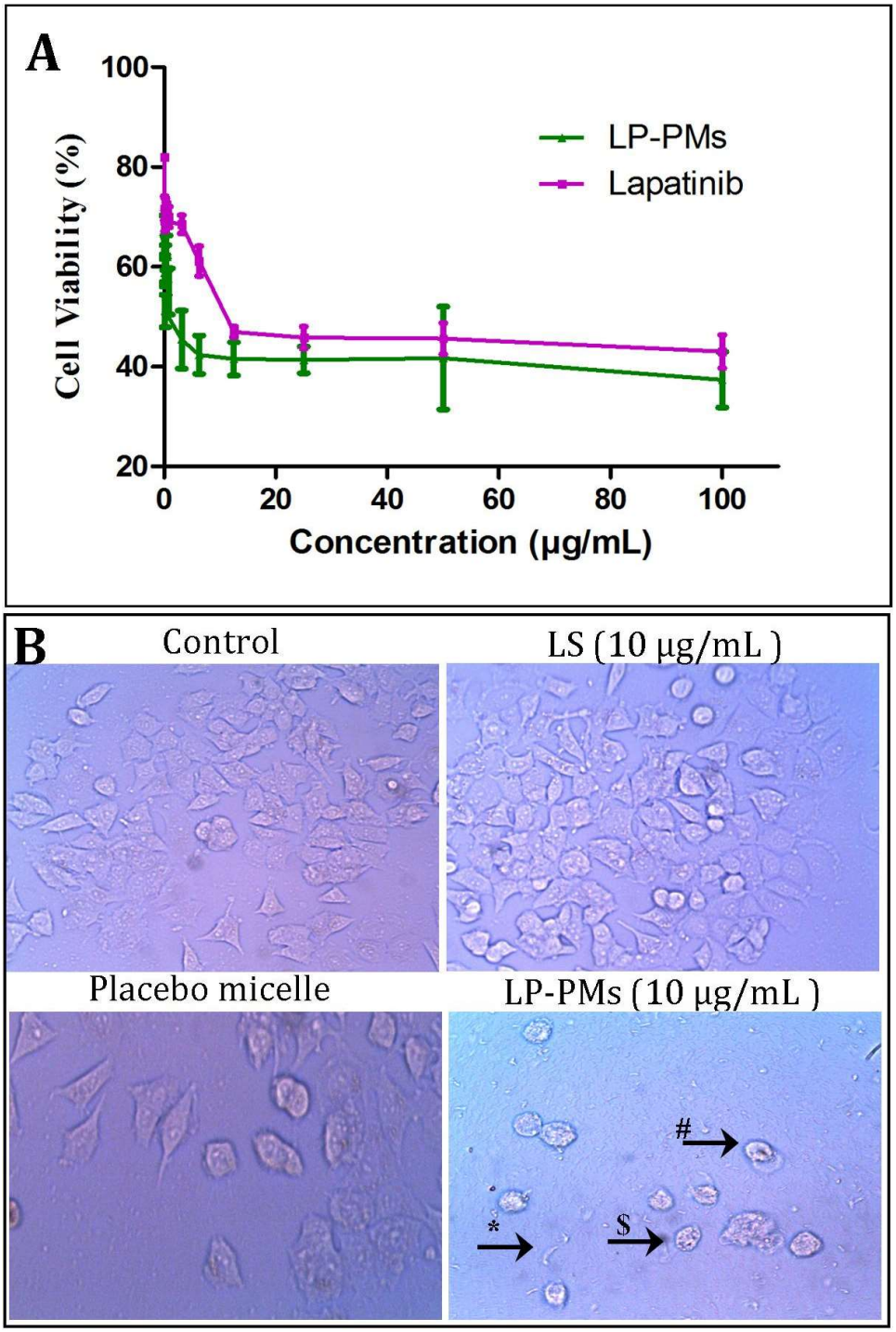

Figure 5.12 *In-vitro* anti-cancer efficacy studies of LP-PMs against SKBr3 breast cancer cell line: (A) Results of percent cell viability by MTT method; (B) microscopic images of SKBr3 cells after treatment with different solutions and LP-PMs

5.2.8 *In-vivo* evaluations

5.2.8.1 Pharmacokinetic studies

The fate of the administered drug in the form of different dosage forms were evaluated by pharmacokinetics studies via oral route for marketed tablets and intravenous route for LS and LP-PMs. The plasma from the collected blood samples from rats of various treatment groups was estimated for drug concentration by HPLC method. The study was conducted upto 48h after drug/ dosage form administration. Figure 5.13 illustrates the mean plasma concentration Vs time profiles of three lapatinib formulations in rats and their corresponding estimated pharmacokinetic parameters are tabulated in Table 5.12.

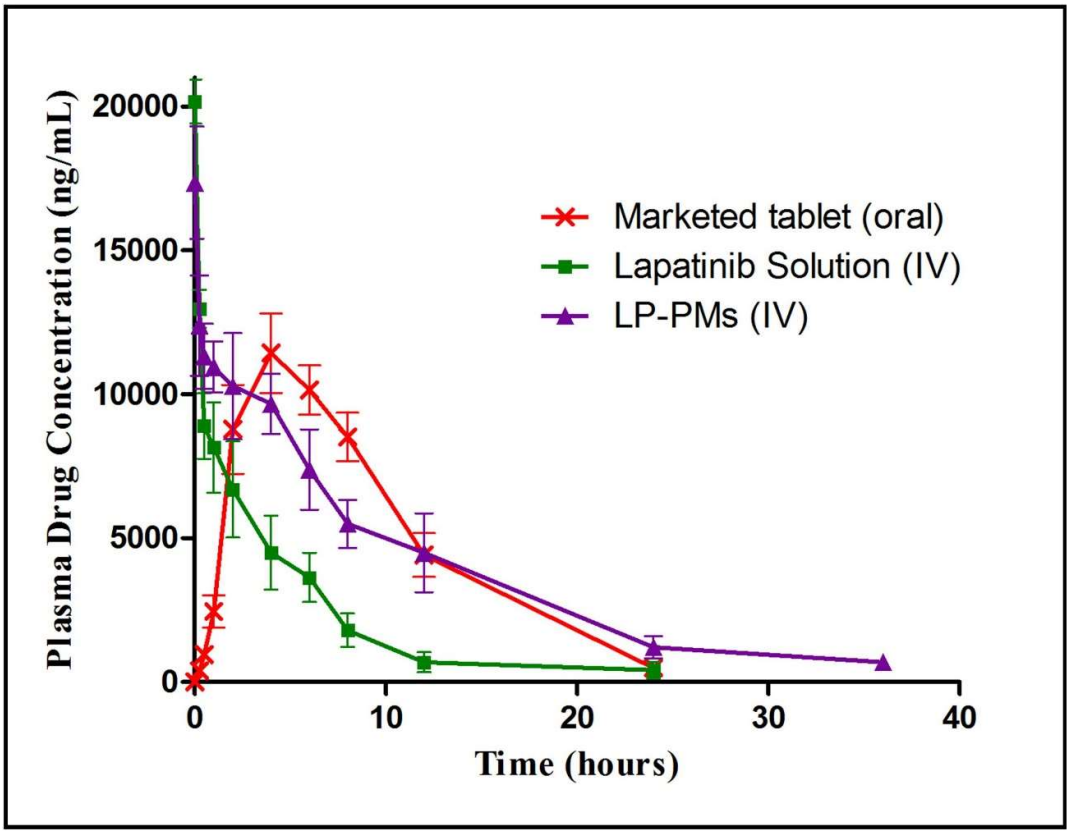

Figure 5.13 Comparative plasma drug concentration profiles of LP-PMs and LS after I.V. administration and marketed tablet after oral administration; data point represents mean ± SEM (n=6)

Table 5.12 Estimated pharmacokinetic parameters of different dosage forms

Groups	Marketed Tablet	LP Solution	LP-PMs
C_{max} (ng/mL)	10229	12968	12389
t_{max} (h)	4.62	-	-
$t_{1/2}$ (h)	3.33	4.95	8.15
MRT(h)	9.26	6.41	11.33
$AUC_{0–48\ h}$ (ng/L*h)	124321	54792	138056

The plasma concentration profiles of marketed tablets demonstrated a slow initial absorption phase. The peak plasma concentration was observed around 4h that was followed by rapid elimination of LP from blood. For the rat group treated with LS, initial higher concentration was evidenced due to instant availability of free drug via IV administration. However, it was rapidly eliminated from the circulation, as shown in **Figure 5.13.** Though LS had eliminated with faster rate, the plasma concentration of LP remained higher than that in marketed tablet treated group.

Further, the initial concentration of LP in LP-PMs group was lower than in LS-treated group. It might be due to the release of drug from surface of LP-PMs and small extent of drug from LP-PMs core. Rapid clearance of the LP was followed by comparatively slower clearance after 30 min evidenced by the decrease in the slope of curve after 30 min. The effect can be attributed to slower drug release by diffusion from the core of LP-PMs as compared to initial 15 min and the commencement of the sustained release phase of the drug. The clearance of drug was then followed upto 36 h but at each time interval the LP concentration was higher than that observed in LS treated group. The higher concentration of LP indicated retarded elimination rate of drug as compared to LS group and can be attributed to encapsulation of drug inside the micelllar core causing its slower release. Thus, the formulation was able to maintain drug concentration at higher plasma levels. The prolonged mean residence time (MRT),

enhanced elimination half-life ($t_{1/2}$), and enlarged AUC evidenced that formulated LP-PMs possessed a prolonged blood circulation time than the LS, which was rapidly cleared from blood. The hydrophilic corona of micelles led to reduction in uptake by the reticuloendothelial system and clearance.

Prolonged circulation of LP-PMs was evidenced not only by 0.64 and 1.45 fold increase in half-life but also by 1.77 and 1.22 fold improved MRT as compared to LS and marketed tablet, respectively. Further, 1.52 (LS) and 0.11 (MT) fold increase in AUC of LP-PMs suggested the higher bioavailability of drug when administered by IV route. Mechanism behind these observations could be the sustained LP release from the LP-PMs from its core and reduction in clearance of drug. Conclusively, it can be said that incorporating LP in micellar form could significantly enhanced its systemic circulation and bioavailability, which could be the basis for delivering the drug to tumor tissues and enhancing its anti-tumor efficacy.

5.2.8.2 Pharmacodynamic studies

The *in-vivo* anti-cancer efficacy of prepared micelles was evaluated using the ectopic xenograft mice model having *in-situ* SKBr3 tumors. The treatment was carried out for 28 days following which the tumors were excised and the volume of tumor tissue was measured [**Figure 5.14(A)].** The reduction in the tumor size and rate of inhibition [**Figure 5.14(B)**] in the LP-PMs ($p<0.001$) and marketed formulation ($p<0.05$) treated group was significantly higher as compared to the control group animals. In the LS treated animals, tumor growth inhibition was 5.66 ± 3.64% post treatment, whereas the marketed oral formulation caused 23.09 ± 8.56% inhibition of tumor growth that is significant ($p<0.05$) in comparison to LS group. The highest activity was seen in LP-PMs treated animal group with 44.83 ± 5.64 % tumor growth inhibition, which was significantly higher compared animal groups treated with LS ($p<0.001$) and marketed

tablet ($p<0.05$). Moreover, significant difference in the volume reduction after treatment with LP-PMs was evidenced when it is compared with LS group ($p<0.001$) and marketed tablet group ($p<0.01$); as illustrated in **Figure 5.14(C).**

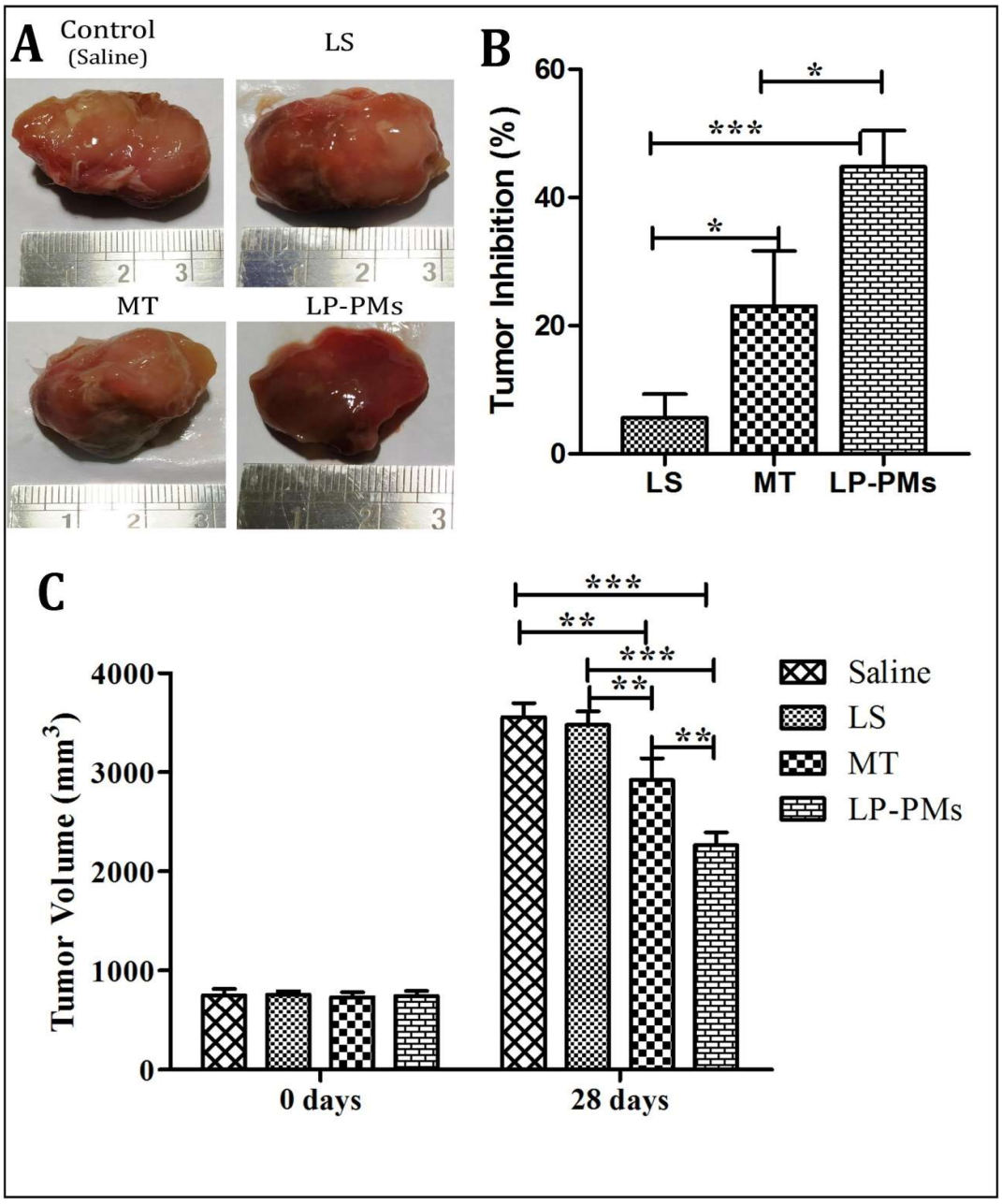

Figure 5.14 *In-vivo* anticancer efficacy of LP-PMs showing (A) tumor photographs; (B) percent inhibition of tumor growth post-treatment; (C) tumor volume.

The nanosized micelles (<100 nm) tend to accumulate in the tumor tissue by default owing to the leaky vasculature in the tumors (known as EPR effect). Also, the encapsulation of the drug inside the micellar core protects the drug against losses due to plasma protein (albumin) binding during circulation. Thus, the dose of the prepared micellar formulation was 10 times lower than the marketed oral tablets which therefore, prove to be the effective treatment for breast cancers. Though the route of administration of the drugs had been changed, with the help of nanomicellar drug carriers, the anti-cancer efficacy of the drug can be retained along with reduction in the dose of highly hydrophobic drug. In conclusion, it can be said that LP-PMs could serve as a booster for the therapeutic potential of LP.

5.2.8.3 Histopathological Studies

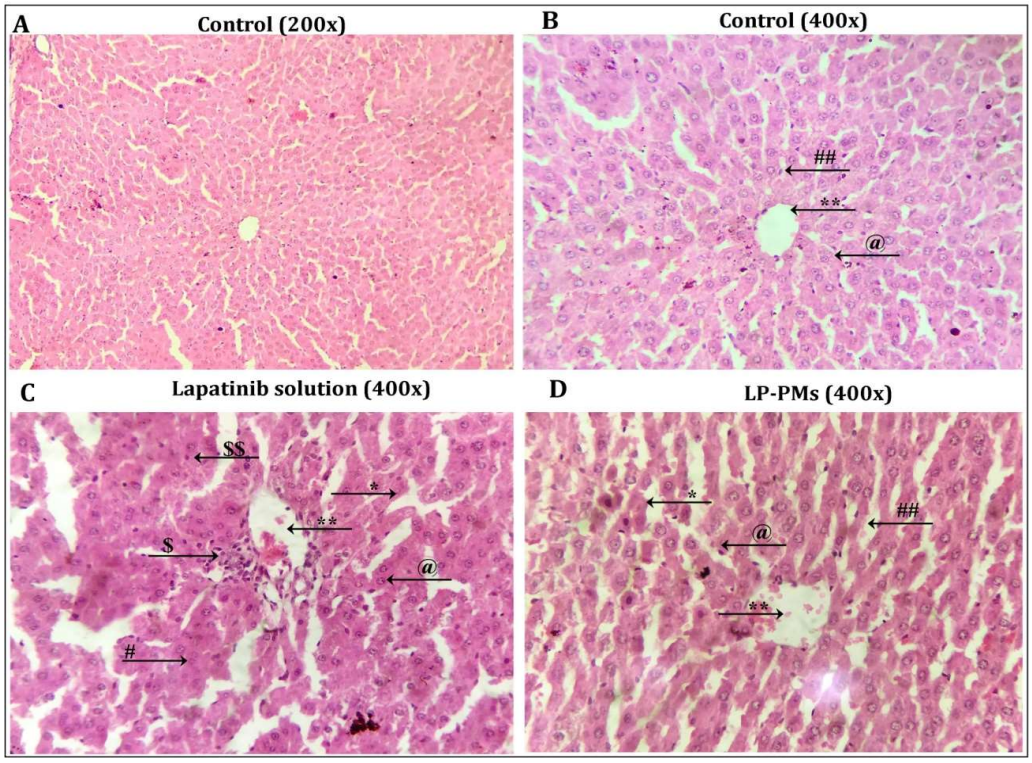

Figure 5.15 The microscopic images of liver sections after staining with H & E stains: (A) normal liver parenchyma (200x) from control group; (B) shows a magnified view of (A) (400x); (C) revealing severe liver damage in group treated with lapatinib solution (400x); (D) depicting very mild toxicity in the group treated LP-PMs (400x).

Hepatotoxicity is one of the significant side-effect of tyrosine kinase inhibitor family of anti-cancer drugs of which LP is a member [Castellino et al. 2012, Spraggs et al. 2013]. The hepatotoxicity is determined by observing the significant changes in the normal hepatocytic parenchyma of the hepatic lobules. The changes include enlargement or dilatation of sinusoidal spaces, hydropic degeneration, vacuolization of hepatocytes, disruption of lobular organization, infiltration of inflammatory cells like neutrophil as a sign of inflammation, and necrosis, etc. [Demirci et al. 2012].

The normal parenchyma of hepatocytes (denoted by @) and converging histological organization of hepatocytes with central vein (denoted by **) that can be seen from **Figure 5.15** (A and B). Additionally, Kupffer cells (denoted by ##) were intermittently scattered and identified by their characteristic spindle shaped nuclei. The group treated with oral lapatinib solution showed significant toxicity to liver as depicted from **Figure 5.15** (C). It is evidenced by the symptoms like sinusoidal dilatation (denoted by *) and disorganization of hepatocytes and sinusoidal spaces (denoted by #). Also, significant inflammation around central vein was confirmed by the presence inflammatory cells (denoted by $) with fewer hepatocytes undergoing necrosis and degeneration of their nuclei (denoted by $$). Further, as seen from **Figure 5.15** (D), the absence of most of the toxicity symptoms except milder dilatation of sinusoidal spaces in perilobular space revealed that the LP-PMs were safe as compared to lapatinib solution; however very milder hepatotoxicity did exist comparing to normal liver.

Lapatinib primarily metabolized by CYP 3A4 and 3A5 enzymes in liver. The LP is metabolized in various metabolites primarily dealkylated phenolic metabolites that are reported and potentially related to hepatotoxicity [Spraggs et al. 2013]. The absorption of LP from GIT post-oral administration follows portal circulation and, thus, the liver is the exposed to almost all the amount of LP absorbed in blood resulting in maximum hepatotoxicity. One of the rationales of the study was to avoid the exposure of liver of

LP in above-said pathway by I.V. administration. Additionally, the encapsulation of the drug inside the core of the micelle could significantly reduce the free LP in blood circulating through liver, thus, explained the significantly reduced toxicity to liver and is evidenced from **Figure 5.15** (D).

5.3 Development and evaluation of Lapatinib-loaded Binary Micelles (LP-BMs)

5.3.1 Formulation of LP-BMs

LP-BMs were fabricated by mixing both the amphiphilic polymers viz. SOL and SHS in various combinations as given in **Table 5.13.** To predict the effect of different levels of each contributing polymers, various combinations were chosen while each of the LP-BMs preparations contained same amount of LP. LP-BMs 5 (having higher EE) was then lyophilized and was stored. The lyophilized LP-BMs 5 was then evaluated for various parameters. The results are summarized in **Table 5.13.**

Table 5.13 Composition of LP-BMs and the results of evaluations

Code	Ratio of SHS:SOL	EE (%)	Total	DL (%)
LP-BMs 1	5:0	71.59±2.88	120	11.93±0.48
LP-BMs 2	4:1	77.23±2.35	120	12.87±0.39
LP-BMs 3	3:2	81.42±1.06	120	13.57±0.18
LP-BMs 4	2:3	83.56±2.99	120	13.93±0.50
LP-BMs 5	1:4	89.45±1.98	120	14.91±0.33
LP-BMs 6	0:5	82.24±2.34	120	13.71±0.39

EE = Entrapment efficiency; DL = Drug loading; the values are expressed as mean ± standard deviation, n=3.

5.3.1.1 Effect on encapsulation efficiency and drug loading

The EE and DL of the various batches of LP-BMs are given in **Table 5.13**. As LP-BMs 5 was found to have higher EE and DL, the formulation is considered for other evaluations. The results of EE and DL showed that the increase in the concentration of SOL in the combination resulted in higher encapsulation of drug. This effect may be attributed to the branched structure of SOL in contrast to linear structure of SHS.

Therefore, the increased contribution of 3-dimentional branched structure might have resulted in the obstruction to the drug release and during the hydration phase more and more drug might have entrapped in the micellar structure. Moreover, more entanglement of branched parts as well as their enforcement by some portion of linear SHS might have resulted in high EE of LP-BMs 5 than LP-BMs 6.

5.3.2 Physicochemical characterization

5.3.2.1 Particle size and polydispersity index analysis

LP-BMs 5 micellar dispersion was evaluated for the determination of hydrodynamic diameter by DLS analysis and results are shown in **Figure 5.16(A).** The diameter of micelles was found to be 93.53 ± 3.56 nm with a PDI of 0.22 ± 0.02. The graphical illustration shows the Gaussian distribution around the average value of diameter of micelles. The lower PDI values ensured their monodispersivity. The size of LP-BMs was found to be less than 200 nm; implying their suitability for EPR effect *in-vivo*.

5.3.2.2 Zeta potential

The zeta potential of the LP-BMs was -12.30 mV; as shown in **Figure 5.16**(B). The –OH functional groups of PEG moieties in the molecule of SOL and –OH moieties at 12^{th} carbon of SHS with its free –OH at esterified end conveyed a negative zeta potential to LP-BMs and also in comparison to positive zeta potential of LP-PMs [Jin et al. 2015]. Additionally, SHS consists of about 30% free polyethylene glycol with its two free –OH at both ends which might have contributed to the observed negative zeta potential of micelles [BASF].

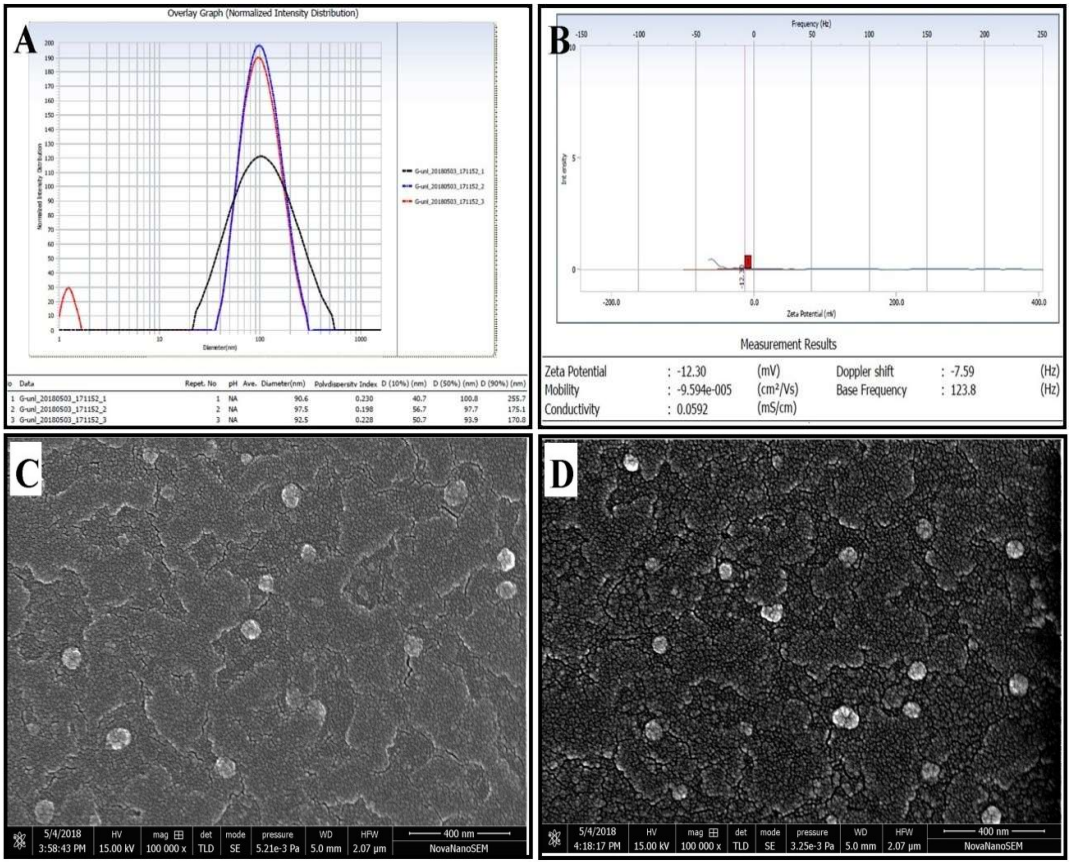

Figure 5.16 (A) Histogram showing the hydrodynamic diameter and (B) zeta potential of LP-BMs; (C and D) High resolution- scanning electron microscopic image showing spherical shape of LP-BMs and lyophilized LP-BMs, respectively.

5.3.2.3 High Resolution-Scanning Electron Microscopy

High-resolution scanning electron microscopy (HR-SEM) was used to visualize the morphology of LP-BMs. **Figure 5.16**(C and D) demonstrates the spherical shape of LP-BMs. The LP-BMs had an average diameter ranged between 62–94 nm with an average of 75.37±13.87 whereas lyophilized LP-BMs had PS between 58–81 nm with an average diameter of 67.14 ± 10.19 nm. However, the lower values of diameter in HR-SEM observations were because of drying of LP-BMs in sample preparation process, as discussed earlier. This fact supports the hypothesis of selective and passive targeting of the prepared delivery system for tumours.

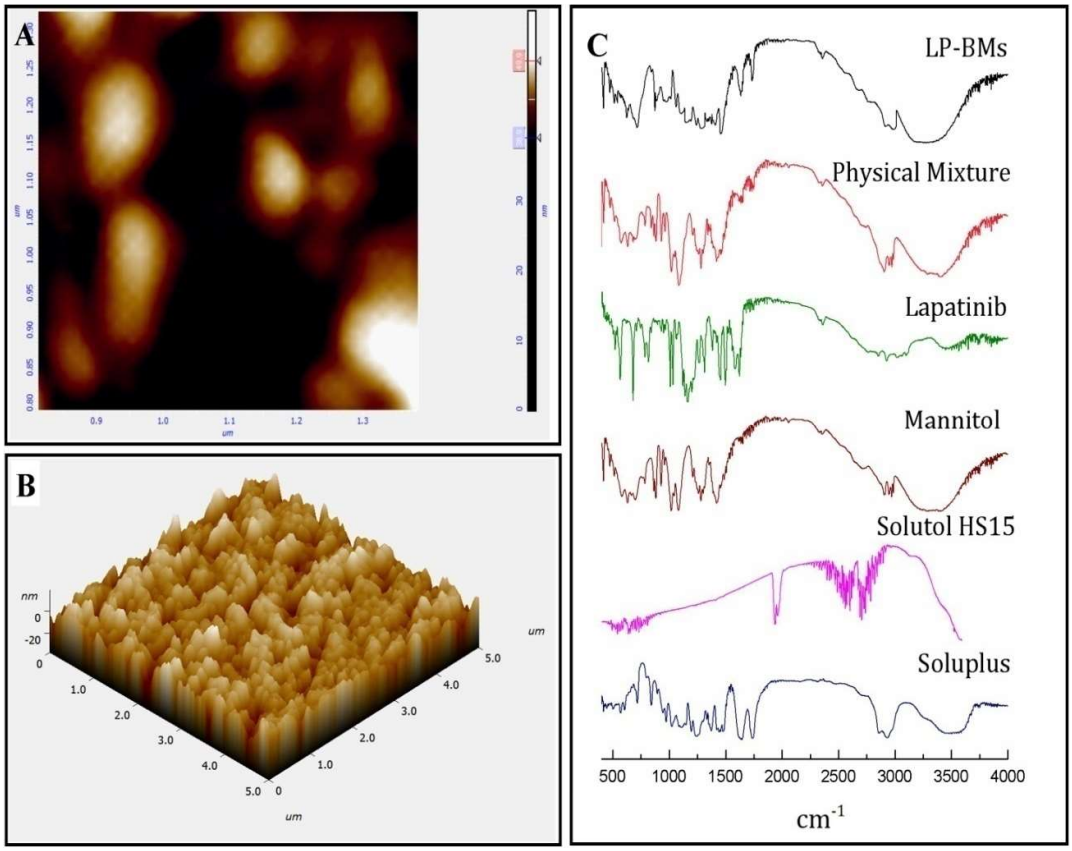

Figure 5.17 (A and B) scanning probe microscopic images showing 2-D and 3-D morphology, respectively; (C) FT-IR spectra of LP-BMs and pharmaceutical excipients

5.3.2.4 Scanning Probe Microscopy

The roughness of surface of the micelle film was visualized by SPM, and the images revealed nearly spherical shape and smooth surface of micelles which can be seen from **Figure 5.17** (A). As seen from **Figure 5.17**(B), an average peak-to-peak height was 60 nm in 3-dimensional view, which may be similar to apparent diameter of the micelles. The results of SPM evaluation were in good agreement with those observed in HR-SEM studies. The drying of the micelles during spin coating for sample preparation might have resulted in lower observed values of diameter than the hydrodynamic diameter as observed in DLS [Chen et al. 2016].

The results of DLS, HR-SEM and SPM evaluations indicated better tumor targeting capability of the prepared LP-BMs having their size well below 100 nm. Additionally,

their spherical shape and smooth surface, characterized by SPM, may facilitate their transit through blood stream and could minimize opsonization and adsorption to the proteins.

5.3.2.5 Fourier Transform Infra-red (FT-IR) study

The spectra of SHS showed a characteristic peaks at 2995 cm^{-1} indicating C–O stretch, as seen from **Figure 5.17** (C) [Al Kayal et al. 2015]. The physical mixture showed no extra peaks. However, the LP-BMs spectra demonstrated broadening of band between 3300 – 3600 cm^{-1}.

The physicochemical interaction of the ingredients and their compatibility was studied by the FT-IR spectra of excipients, LP-BMs and the physical mixture. Physical compatibility of drug existed with all the excipients and was evidenced by conserving all the characteristic peaks in physical mixture. However, the LP-BMs showed broadening of bands between 3300–3600 cm^{-1} indicating existence of intermolecular hydrogen bonds; confirming our results with previous reports [Knop et al. 2011]. That might be one of the reasons for higher encapsulation of LP and to sustain the LP release from LP-BMs.

5.3.2.6 Energy dispersive X-ray Analysis (EDX)

The EDX analysis was employed to verify the elements present in LP-BMs. The presence of carbon, oxygen and hydrogen with fluorine and sulfur was evidenced from **Figure 5.18 (A).** An EDX spectrum of LP-BMs depicts the typical constituents of LP and absent in SOL and SHS molecules. The findings demonstrated that LP was successfully encapsulation inside the micelles, whilst some of the drug was also present on the surface of the LP-BMs. It was indicated by very small peaks of sulfur and fluorine in the EDX spectrum on LP-BMs.

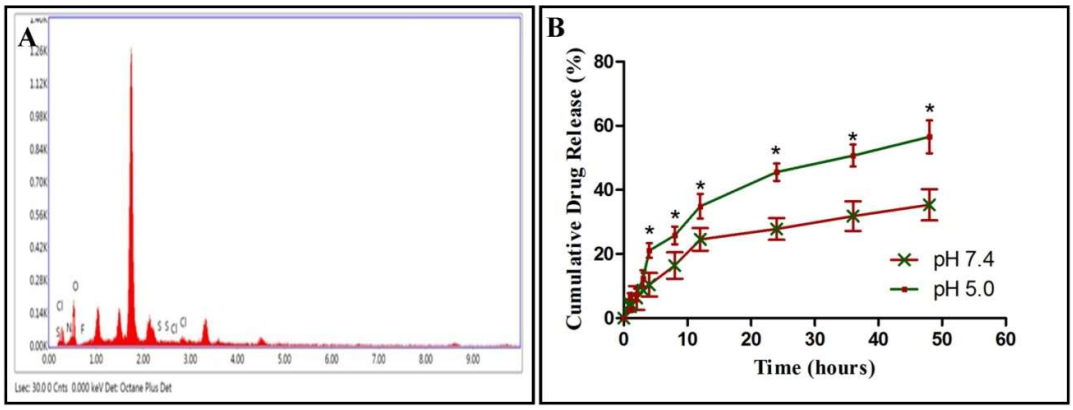

Figure 5.18 (A) EDX spectra of LP-BMs; (B) *In-vitro* drug release profile of LP-BMs in release media of pH 5.0 and pH 7.4

5.3.3 *In-vitro* Evaluations

5.3.3.1 Drug release studies

The comparison of drug release profiles in different pH media is illustrated in **Figure 5.18(B)**. In the release media of pH 7.4, approximately 28% of LP had been released within first 24h; followed by the slow release phase and over 48h only 35% of the drug was released. In contrast to that, nearly 46% and 57% of drug was found to be released in the release media of pH 5.0 at the end of 24h and 48h, respectively. Different kinetic models were investigated and fitted with the above drug release data, and Higuchi model was observed to be best suitable model explaining drug release. Moreover, 0.474 and 0.453 were the values of the Peppas exponent '*n*' at pH 5.0 and pH 7.4, indicating LP release by Fick's diffusion.

The dialysis bag method was employed for *in-vitro* release evaluation of LP-BMs and sink condition was maintained by adding Tween® 80 to release media. The results corroborated that the LP-BMs could sustain the release of drug from the micelles. The effect can be attributed to the slower diffusion of drug from the tortuous pathways formed by entanglement of chains of polymers in 3-D structure of micelles which might

have resulted in the obstruction to the drug release [Li et al. 2011b, Senapati et al. 2018]. Moreover, the comparatively higher drug release at pH 5 than pH 7.4, simulating tumour and blood environment, respectively, suggested their selective drug delivery at intended site [Senapati et al. 2018]. The sustained effect might show the possibility of reduction in the effective dose of LP. Further, the drug release data were best fitted in Higuchi model which suggested the drug release followed diffusion process.

5.3.3.2 Haemocompatibility study

For evaluation of hemocompatibility, whole blood was treated with LP-BMs or LP solution (LS) at the four different concentrations. The difference in induced hemolysis was non-significant at lowest concentration of drug in solution and micellar form. But the hemolysis was increased in LS treated group as the concentration of drug increased. As the concentration of drug increased to 1 and 1.5 µg/mL, the significant ($p<0.05$) difference was found in LS and LP-BMs treated group. At the highest concentration, LP-BMs showed significantly ($p<0.01$) hemolysis than LS treated group, as illustrated graphically in **Figure 5.19**(A). Thus, the experimental findings revealed that LP-BMs or LS did not induce significant hemolysis, i.e., below a limit of one percent at the experimental LP concentration range.

The formation of emboli or significant RBC hemolysis is the indications of incompatibility of dosage form with blood components, raising the risk to the patient. [Mittal et al. 2019]. As hemolysis induced by LP-BMs was less than one percent, it was concluded that the prepared LP-BMs are safe for I.V. administration. The micellar encapsulation of LP inside the core of micelles might be the possible reason for observed reduction in hemolysis in case of treatment with LP-BMs, as compared to LP solution.

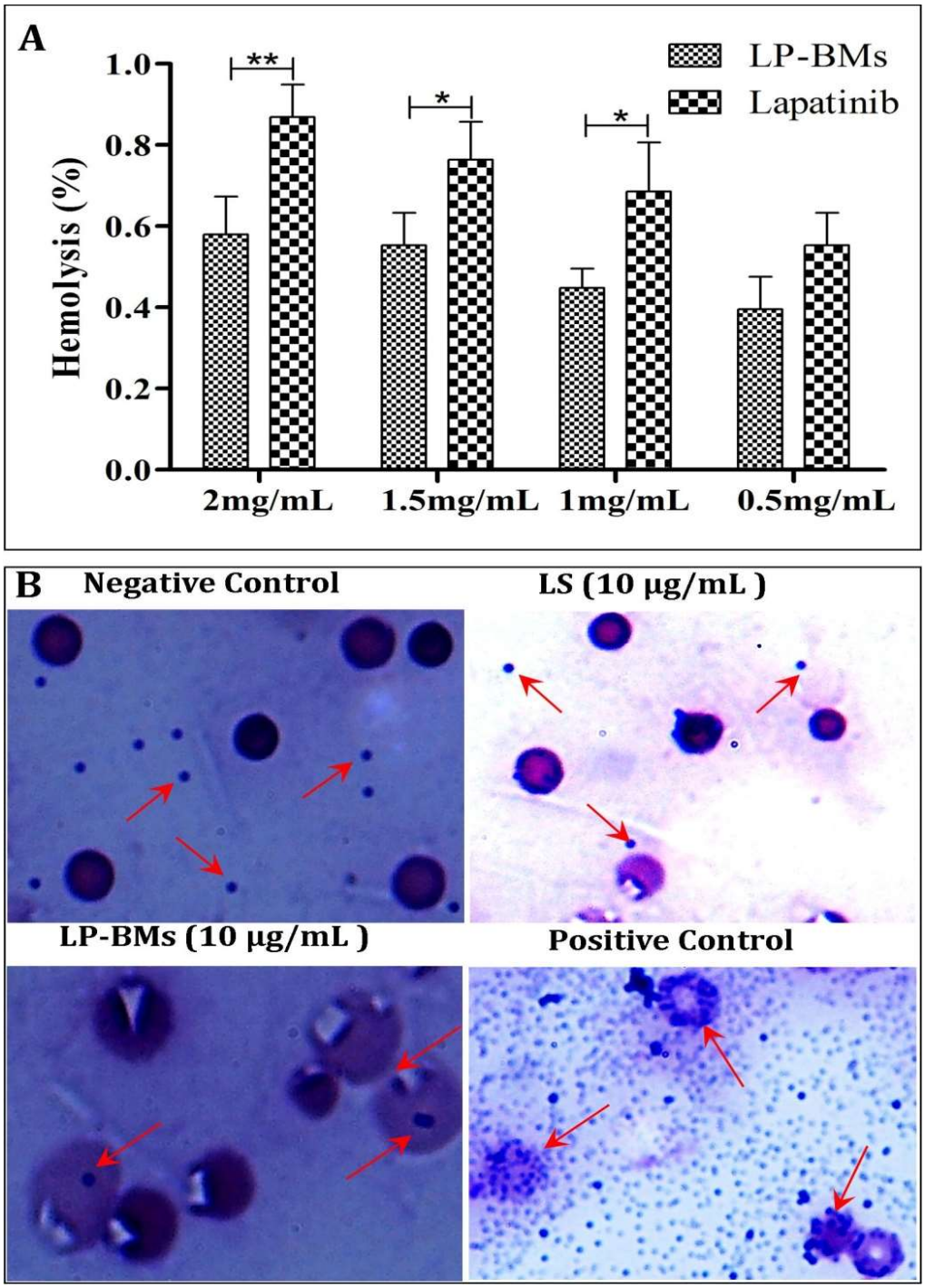

Figure 5.19 (A) Hemocompatibility of LP-BMs in terms of percent hemolysis; (B) platelet aggregation study illustrating no platelet aggregation after treatment with LP-BMs

5.3.3.3 Platelet aggregation studies

Discoid shaped platelets were widely dispersed all over the FOV and the platelet aggregation was observed neither in the control, LS nor in the LP-BM–treated blood samples; as revealed from **Figure 5.19**(B).

The induction of aggregation of platelets in the blood pool is a deleterious indication for an I.V. Dosage form which can be fatal to patient. Thus, the LP-BMs were evaluated and did not cause any platelet aggregation with maintained morphology of platelets, confirming the hemocompatibility of LP-BMs [Mittal et al. 2019]. Our findings thus evidenced that LP-BMs were safe and can be served as a desirable nanocarrier for I.V. route of administration.

5.3.4 Stability Studies

The LP-BMs dispersion and lyophilized LP-BMs stored under two conditions of temperature and relative humidity for estimating the effects on their stabilities. The LP-BMs stored at both the conditions did not show any significant ($p< 0.05$) change in the EE at each sampling time. The results for EE before and after the sampling time as well their respective estimated shelf life are tabulated in **Table 5.14**. Further, the shelf life plots were prepared using EE and Minitab® version 7, as shown in **Figure 5.20**.

At 3 months, a significant enhancement of the stability was observed in dispersion phase at 30°C ± 2°C/65% RH ± 5% RH and the estimated shelf life of 8 months, as compared to LP-PMs in dispersion form that were aggregated within 3 months. Further, the results corroborated that the lyophilization resulted in transformation of liquid dispersion to solid powder form that markedly enhanced its stability especially at 30°C ± 2°C/65% RH ± 5% RH upto 15 months. On the other hand, lyophilized LP-BMs showed highest shelf-life of 19 months. Thus, the refrigerated condition could be the best suitable condition for storage of lyophilized LP-BMs, although their stability at

room temparature was as per expectation.

Table 5.14 Results of evaluations before and after stability studies.

	Conditions	**30°C ± 2°C/65% RH ± 5% RH**	**5°C ± 3°C**
	Time (month)	**EE (%)**	**EE (%)**
LP-BMs	0	89.45 ± 1.98	89.45 ± 1.98
	3	86.86 ± 4.58	87.59 ± 5.6
	6	84.50 ± 5.9	85.77 ± 4.77
Estimated Shelf-life (months)		8	13
Lyophillized LP-PMs	0	88.86 ± 5.77	88.86 ± 5.77
	3	87.77 ± 4.37	87.95 ± 4.64
	6	86.50 ± 3.83	86.86 ± 4.92
Estimated Shelf-life (months)		15	19

*All the results are mentioned as mean ± standard deviation, n=3.

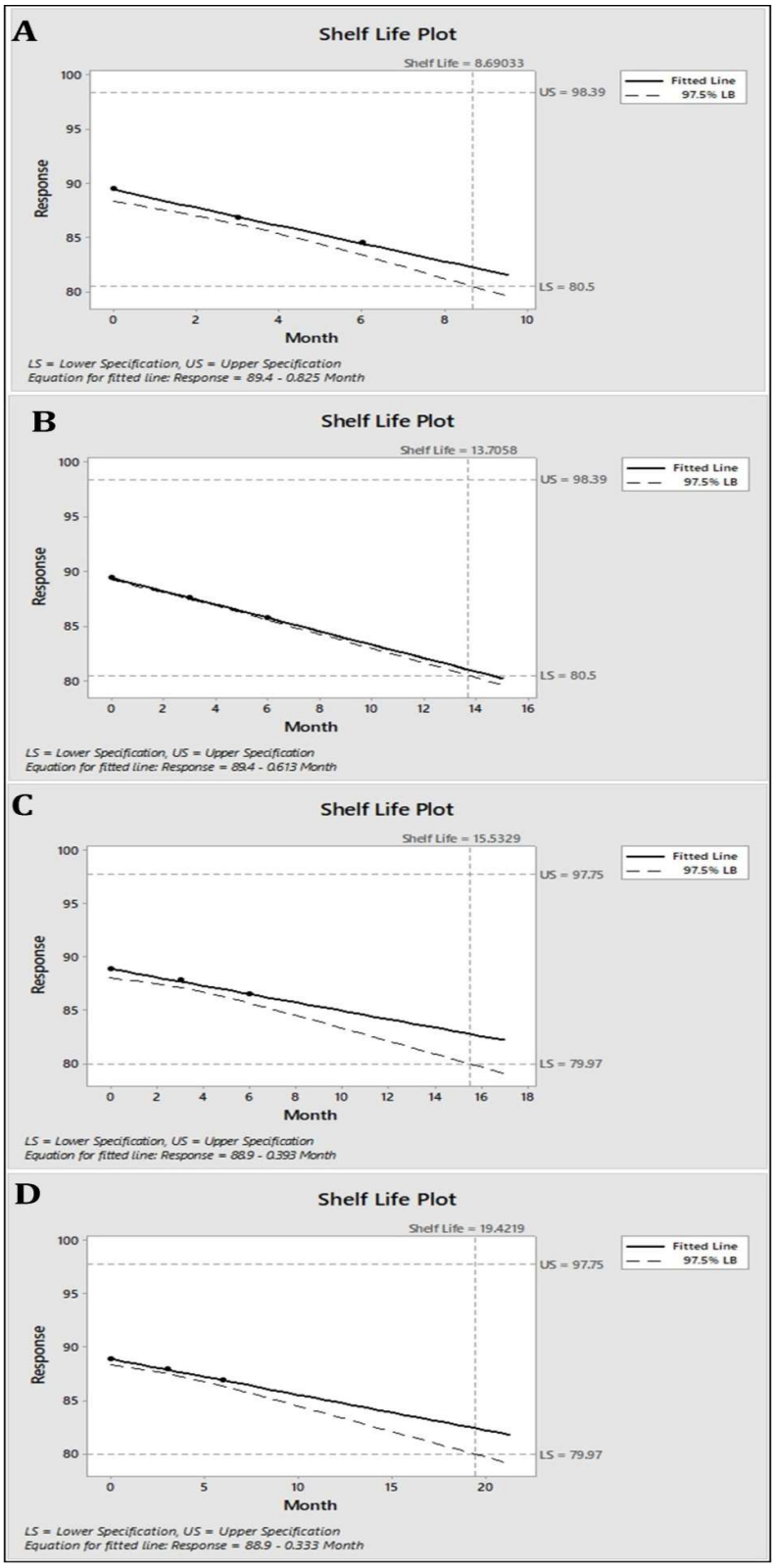

Figure 5.20 Shelf life plots of LP-BMs: (A) in dispersion form at 30°C ± 2°C/65% RH ± 5% RH; (B) in dispersion form at 5°C ± 3°C; (C) in lyophilized form at 30°C ± 2°C/65% RH ± 5% RH; (D) in lyophilized form at 5°C ± 3°C

5.3.5 *In-vitro* screening of anticancer efficacy

5.3.5.1 Cell Culture

For the present studies, SKBr3 were selected, in particular, for *in-vitro* evaluations. SKBr3 barest cancer cell line is characterized by HER2 overexpression [Greenshields et al. 2019, Jeong et al. 2015] and can serve as best for present study.

5.3.5.2 Cytotoxicity assay

Figure 5.21(A) demonstrates the cell viability and inhibition of proliferation of SKBr3 cells by LS and LP-BMs, determined by MTT assay method. The observed IC_{50} of LP-BMs and LS were 1.22 and 8.19 µg/mL, respectively, for SKBr3 cancer cell line.

The MTT-based assay was performed on SKBr3 cancer cells to evaluate the anticancer efficacy of LP-BMs. The significantly lower IC_{50} values of LP-BMs revealed better anticancer efficacy than free drug against HER2 positive cell lines. Hence, the micellar encapsulation of LP could, indeed, improve the cytotoxicity of LP to the breast cancer cells.

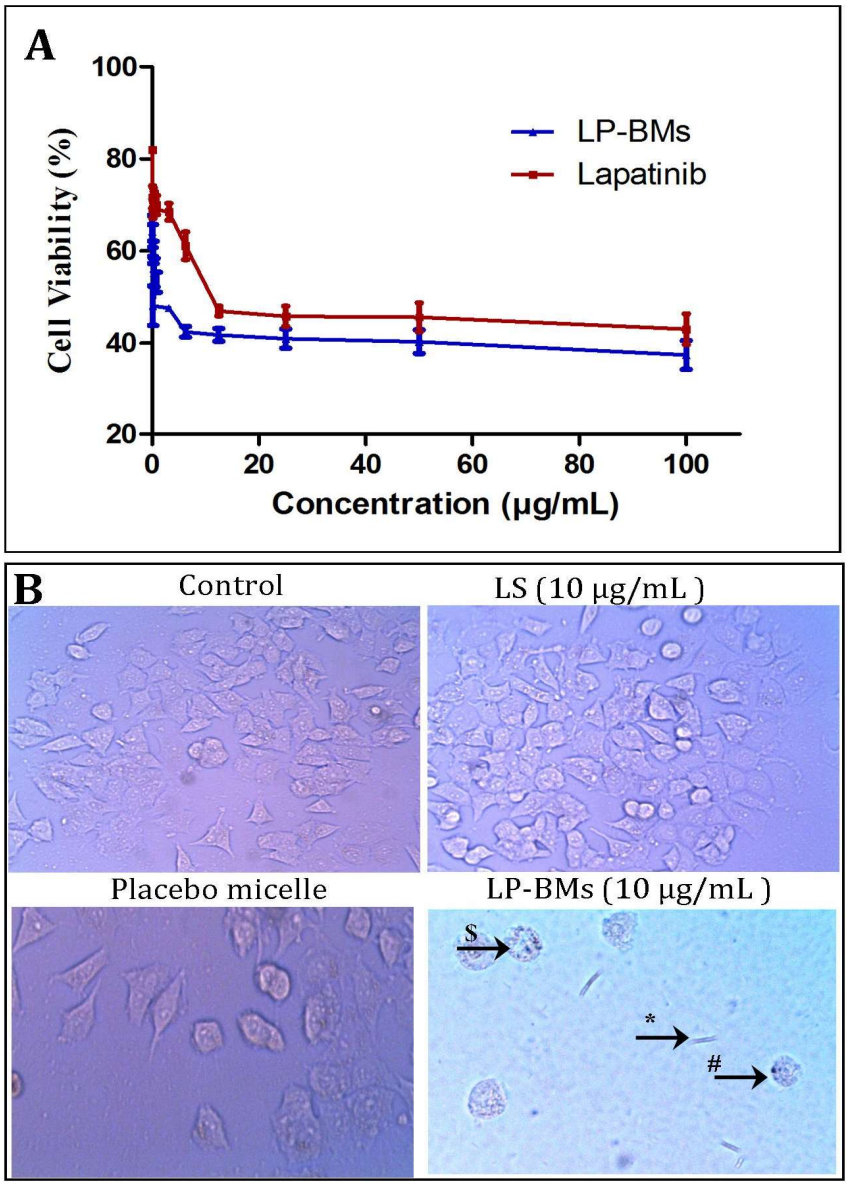

Figure 5.21 *In-vitro* anti-cancer efficacy studies of LP-PMs against SKBr3 breast cancer cell line: (A) Results of percent cell viability by MTT method; (B) microscopic images of SKBr3 cells after treatment with different solutions and LP-BMs

5.3.5.3 In-vitro anti-cancer efficacy studies

SKBr3 were treated with different solutions and LP-BMs to evaluate the cytotoxicity to cells. **Figure 5.21**(B) reveals the morphological alterations in SKBr3. The untreated or control SKBr3 cells retained their inherent morphology. The cells treated with placebo micelles also did not show any cytotoxic effect. Further, the signs of cytotoxicity to the

cells treated with LP-BMs and can be seen **Figure 5.21**(B). The cytotoxicity was evidenced by presence of numerous smaller rounded cells (#), granular cytoplasm ($), and a few cells showing loss of confluence (*) in the FOV.

The morphological changes induced in cells after treatment with the drugs indicates cytotoxicity. These morphological changes consisted of either shrinking of cytoplasmic contents and more granular appearance indicating chromatin shrinkage or nuclear segmentation [D'Suze et al. 2010] and the circular cell structure due to cytoplasmic condensation [Buttacavoli et al. 2018, Cancemi et al. 2017]. The cells treated with LP-BMs showed such signs confirming their cytotoxicity to SKBr3 cells. Also, absence of any cytotoxic signs in cells treated with placebo micelle additionally confirmed that the observed cytotoxicity was induced by LP-BMs only. The effect was credited to enhanced delivery of LP to the cells in the micellar form owing to increased solubility and encapsulation of LP.

5.3.6 *In-vivo* evaluations

5.3.6.1 Pharmacokinetic studies

The fate of the intravenously administered drug in the form of LP-BMs was evaluated by pharmacokinetics studies and compared with that of marketed tablets and LS by oral and intravenous route, respectively. The study was conducted upto 48 h after drug/ dosage form administration. Figure 5.22 illustrates the mean plasma concentration Vs time profiles of three lapatinib formulations in rats and their corresponding estimated pharmacokinetic parameters are tabulated in Table 5.15. The estimation of pharmacokinetic analysis was performed by using PK solver add in of Microsoft excel.

The plasma concentration profiles of marketed tablets and their pharmacokinetics was already discussed in section 5.2.8.1.

Further, the group treated with LP-BMs group showed less initial concentration of LP than in LS-treated group and as similar to LP-PMs group. The observed lower concentration in the first 15 min was attributed to the release of drug from the LP-BMs surface and diffusion of drug from LP-BMs core to small extent. The rapid clearance phase was observed within first 15 min, followed by the phase of slower clearance after 30 min. This might be the indication of starting the release of the drug from micelle core and thus the higher availability of the drug in the blood. This phase was then followed by clearance of LP from blood evidenced by the decreased drug concentration at following time intervals. However, the LP concentration was sustained and maintained at higher levels than that observed in LS treated group and slightly higher than observed in LP-PMs group. The sustained release of drug and reduction in rate of elimination might have resulted in observed higher concentration of LP in LP-BMs treated group as compared to LS group and can be attributed to encapsulation of drug inside the micelllar core and slower release of LP from LP-BMs.

Table 5.15 Estimated pharmacokinetic parameters of different dosage forms

Groups	Marketed Tablet	LP Solution	LP-BMs
C_{max} (ng/mL)	10229	12968	12456
t_{max} (h)	4.62	-	-
$t_{1/2}$ (h)	3.33	4.95	9.45
MRT(h)	9.26	6.41	12.94
$AUC_{0–48\ h}$ (ng/L*h)	124321	54792	150932

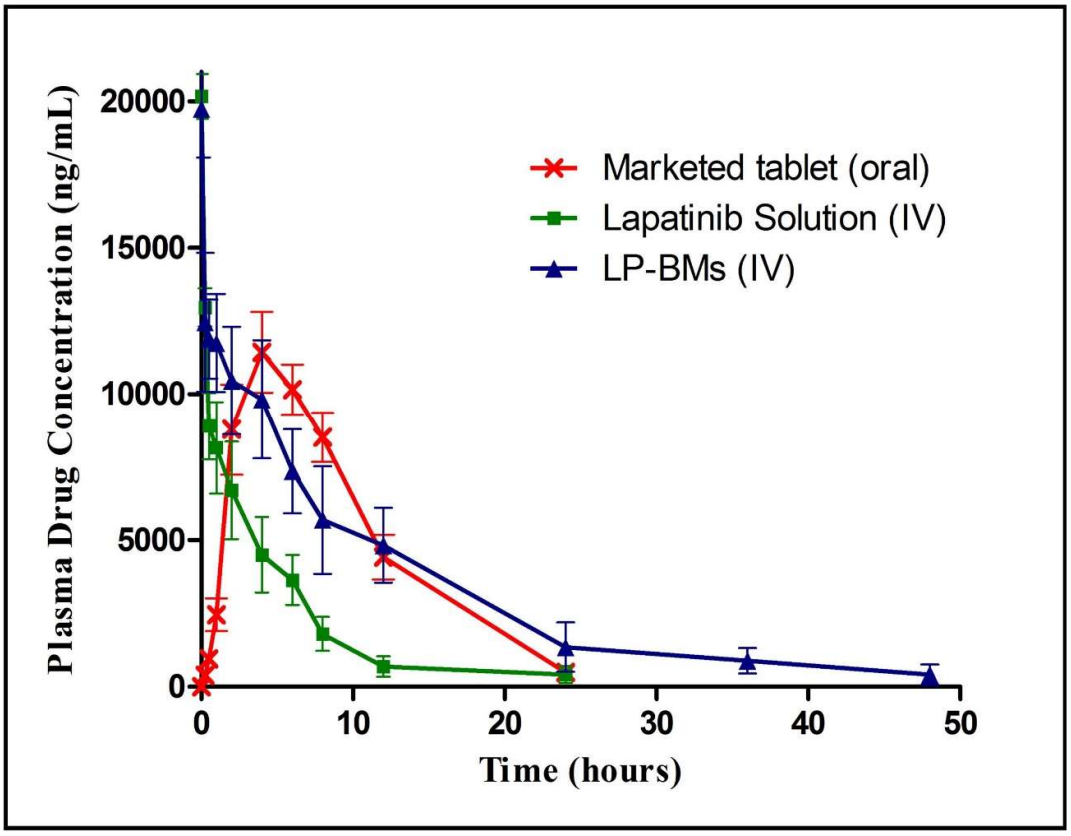

Figure 5.22 Comparative plasma drug concentration profiles of LP-PMs and LS after I.V. administration and marketed tablet after oral administration; data point represents mean ± SEM (n=6)

The circulation half-life of LP in LP-BMs group was found to be 0.91 and 1.85 folds higher than that observed in LS and MT treatment groups, indicating prolonged circulation of drug after LP-BMs administration via I.V. route. It was also supported by the improvement in MRT of LP-BMs to 1.4 and 2.01 times than that observed in case of MT and LS treatment groups, respectively. Further, the higher bioavailability of drug was evidenced by the enhancement of AUC of LP in LP-BMs treatment group to 1.21 and 2.75 fold than observed in MT and LS treatment groups, respectively. All these results indicated that LP-BMs were able to sustain the drug release and was capable for maintaining the higher blood levels of LP. The prolonged mean residence time (MRT), enhanced elimination half-life ($t_{1/2}$), and higher AUC evidenced that formulated LP-

BMs exhibited a prolonged blood circulation time than the LS.

Conclusively, it can corroborated that micellar encapsulation of drug could significantly enhance its systemic circulation and bioavailability, which could further resulted in enhanced delivery of the drug to tumor tissues and enhancing its anti-tumor efficacy.

5.3.6.2 Pharmacodynamic studies

Followed by in-vitro characterization of LP-BMs, we shifted further for their evaluation of *in-vivo* anti-tumor efficacy by employing the ectopic xenograft mice model bearing *in situ* SKBr3 tumors. After 28 days of treatment, the tumors were excised and volume was measured; the results are illustrated in **Figure 5.23.** A significant reduction in growth rate was observed in the group treated LP-BMs as compared to control group while the control tumors were continued to grow at faster rate. The dramatic reduction in the tumor growth rate can be observed after treatment by marketed formulation and LP-BMs. The inhibition of tumor growth by 5.66 ± 3.64% was observed post-treatment by LS whereas 23.09 ± 8.56% inhibition was produced by treatment with marketed oral tablets being significantly higher than LS ($p<0.001$). In case of LP-BMs treated animal group, a marked reduction of 72.60 ± 4.91% inhibition was observed, which was significantly different than that produced in animal groups treated with LS ($p<0.001$) and marketed oral tablets ($p<0.001$).

Further, the highest anti-tumor effect of LP-BMs was evidenced by comparison of the tumor volumes at the end of treatment. The marked reduction in the volume of tumor resulted from treatment of LP-BMs which was significantly ($p<0.001$) different from all the other treatment groups. Moreover, a significant reduction ($p<0.01$) in tumor volume was also observed in the group treated with marketed tablets in comparison to LS treatment group.

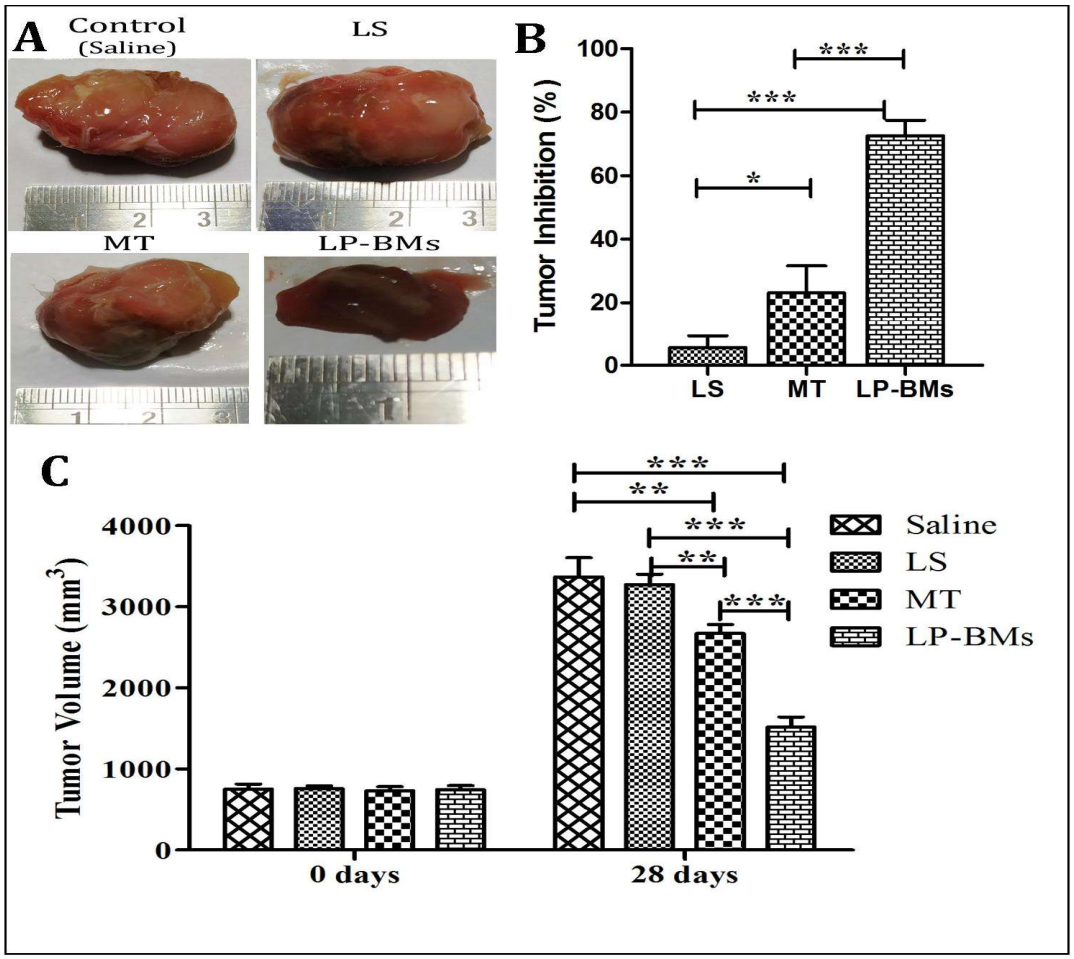

Figure 5.23 *In-vivo* anticancer efficacy of LP-BMs showing (A) tumor photographs; (B) percent inhibition of tumor growth post-treatment; (C) tumor volume.

The enhanced anti-tumor effects could be attributed nanosize, i.e., below 100 nm, of the LP-BMs being a preamble for the EPR effects of nanocarriers enabling their higher tumor accumulation. Another reason might be the encapsulation of drug inside the core of PMs that might have reduced the loss of drug due to plasma albumin-binding during circulation and made it available at tumor site via EPR effect. It is noteworthy to mention that the dose of LP-BMs was 10 times less than marketed oral tablets. Therefore, LP-BMs might prove to be the effective antitumor treatment with much lesser dose as LP-BMs. The observed fact, indeed, confirmed the possibility of dose reduction to a great extent without compromising the anticancer efficacy by the change

of route of administration as well as employing nanomicellar drug delivery system for such a highly hydrophobic drug. Overall, LP-BMs could serve as a better alternate dosage form for IV administration and for better treatment of breast cancer.

5.3.6.3 Histochemical studies

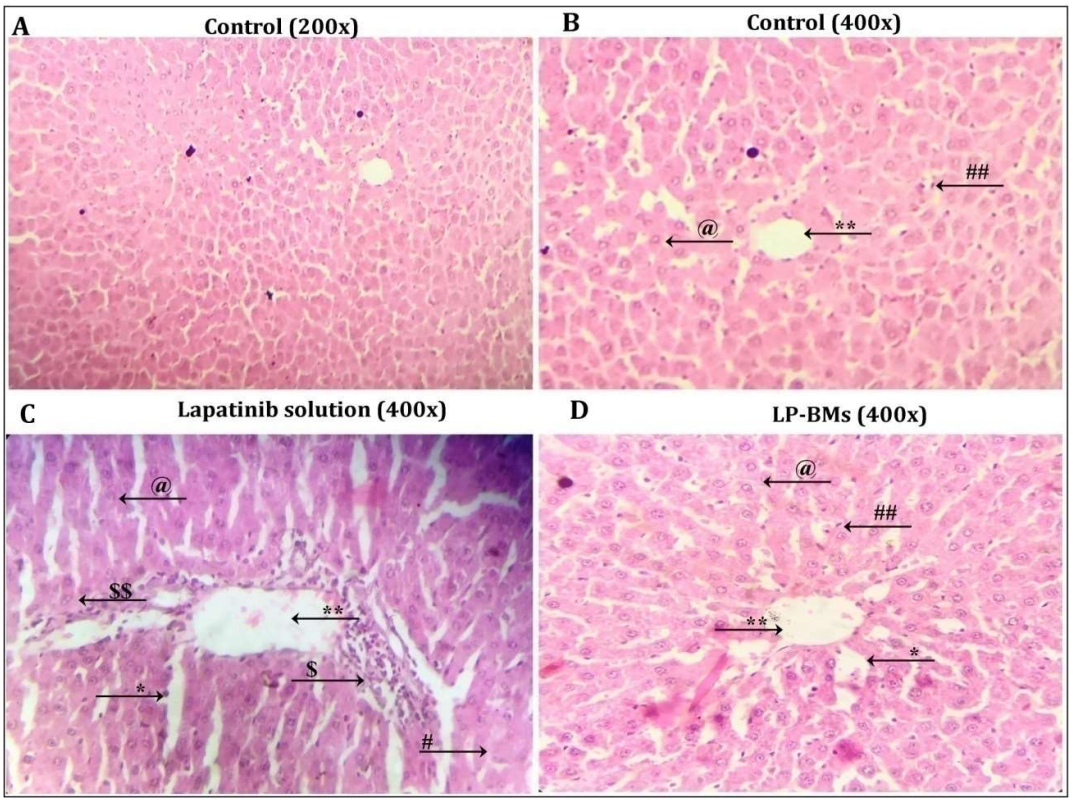

Figure 5.24 The microscopic images of liver sections after staining with H & E stains: (A) normal liver parenchyma (200x) from control group; (B) shows a magnified view of (A) (400x); (C) revealing severe liver damage in group treated with lapatinib solution (400x); (D) depicting very mild toxicity in the group treated LP-BMs (400x).

The normal histology of liver as well as the hepatotoxic changes occurred post-oral administration was previously discussed in 5.2.8.3. The stained section of liver from the rats treated with LP-BMs is shown in **Figure 5.24** (D). The histology almost seems to be similar to normal liver as seen in **Figure 5.24** (B). The lobular structure was intact but dilated (denoted by *) as compared to that in normal liver. The hepatocytes existed in their normal state without any sign of degeneration. The sinusoidal spaces among

hepatocytes were also normal except one or two signs of milder dilatation could be seen around central vein. The condition of liver was even improved in comparison to the treatment with LP-PMs.

The observations and their comparison revealed that LP-BMs can be safe regarding the hetatotoxicity caused by LP. The safety of LP-BMs was attributed to the LP encapsulation inside the micellar core thereby avoiding the contact with hepatocytes during their transit through liver in blood circulation. Conclusively, administration of LP in the form of LP-BMs could remarkably reduce the hepatotoxicity which was observed and reported in previous reports [Castellino et al. 2012, Spraggs et al. 2013].